CZECH TECHNICAL UNIVERSITY IN PRAGUE

Faculty of Nuclear Sciences and Physical Engineering

Department of Physics

Master's Thesis

Triangular particle flow in HYDJET++

Bc. Jana Crkovská

Supervisor: Mgr. Jaroslav Bielčík, Ph. D.

Consultants: Prof. Larissa Bravina, Gyulnara Eyyubova, Ph. D.

Prague, 2015

ČESKÉ VYSOKÉ UČENÍ TECHNICKÉ V PRAZE
Fakulta Jaderná a Fyzikálně Inženýrská
Katedra Fyziky
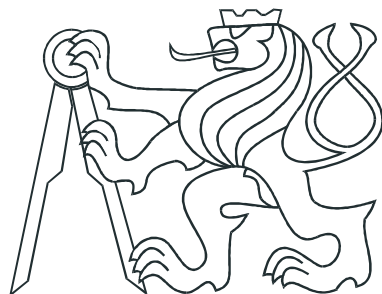
Diplomová práce

Triangulární tok částic v modelu HYDJET++

Bc. Jana Crkovská

Školitel: Mgr. Jaroslav Bielčík, Ph. D.

Konzultanti: Prof. Larissa Bravina, Gyulnara Eyyubova, Ph. D.

Praha, 2015

Prohlášení:

Prohlašuji, že jsem svou diplomovou práci vypracovala samostatně a použila jsem pouze podklady (literaturu, software, atd.) uvedené v přiloženém seznamu.

Nemám závažný důvod proti užití tohoto školního díla ve smyslu 60 Zákona .121/2000 Sb., o právu autorském, o právech souvisejících s právem autorským a o změně některých zákonů (autorský zákon).

V Praze dne 4. května 2015

Jana Crkovská

Title: **Triangular particle flow in HYDJET++**

Author: Bc. Jana Crkovská

Field of study: Experimental Nuclear and Particle Physics

Type of project: Master thesis

Supervisor: Mgr. Jaroslav Bielčík, Ph. D.

Consultants: Prof. Larissa Bravina (University of Oslo),
Gyulnara Eyyubova, Ph. D. (Czech Technical Univeristy in Prague)

Abstract:

Relativistic heavy-ion collisions create systems with energy densities and temperatures high enough for hadronic matter to transfer into quark-gluon plasma (QGP). The later is a state of matter consisting of asymptotically free quarks and gluons. QGP was first observed at the Relativistic Heavy-Ion Collider (RHIC) in 2000.

Collective flow of created hadrons is one of the suggested signatures of the QGP. It was found to be one of the most pronounced signatures and was very thoroughly studied both in theory and in experiment. The flow coefficients studied in heavy-ion experiments are the Fourier coefficients coming from expansion of the invariant differential cross-section into a Fourier series w. r. t. the reaction plane. Triangular flow v_3 originates from event-by-event fluctuations of the overlap zone and in the most central events presents the dominant contribution to anisotropic flow.

Study of triangular flow in Pb+Pb collisions at $\sqrt{s_{NN}} = 2.76$ TeV and in Au+Au collisions at $\sqrt{s_{NN}} = 200$ GeV was performed using HYDJET++ Monte Carlo generator. HYDJET++ combines a soft component, based on parametrisation of relativistic hydrodynamics, together with hard component driving the jets, giving a realistic prediction for vast number of hadron species. The model also enables study of influence of final-state interactions on flow of created hadrons. We have shown that HYDJET++ gives good prediction of triangular flow at LHC energies. There were however issues with calculations at RHIC energies which need to be investigated further. Our study has shown that resonance decays increase the magnitude of the $v_3(p_T)$ distribution at $p_T \geq 1$ GeV/c and shift its maximum to higher p_T. Resonances also drive the triangular flow towards the fulfilment of the number-of-constituent-quark scaling. Jets on the other hand cause scaling violation at the Large Hadron Collider (LHC). Similar effect is not observed at RHIC energies, as at such collisions the jets are significantly less energetic.

Key words: heavy-ion collisions, QGP, collectivity, anisotropic flow, triangular flow, resonance decays, number-of-constituent-quark scaling, LHC, RHIC, HYDJET++

Název práce: **Triangulární tok částic v modelu HYDJET++**

Autor: Bc. Jana Crkovská

Abstrakt:

Při relativistických srážkách těžkých iontů dosahuje systém v nich vzniklý vysokých hustot energie a vysokých teplot. Za takovýchto extrémních podmínek přechází hadrony do stavu takzvaného kvark-gluonové plazmatu (QGP). QGP je stav hmoty, ve které kvarky a gluony nejsou více vázány v hadronech, nýbrž se chovají asymptoticky volně. QGP bylo prvně pozorováno na urychlovači RHIC v roce 2000.

Jedním z možných znaků (tzv. signatur), podle kterých můžeme QGP odhalit, je kolektivní tok částic vytvořených ve srážce. Tok hadronů je jednou z nejlépe prozkoumaných signatur, jak experimentálně tak teoreticky. Z Fourierova rozvoje invariantního diferenciálního účinného průřezu vzhledem k rovině srážky získáme Fourierovy koeficienty v_n, které představují právě jednotlivé koeficienty toky studované v těžkoiontových experimentech. Triangulární tok v_3 pochází z počátečních fluktuací reakční oblasti v jednotlivých událostech a představuje nejdůležitější příspěvek k anisotropickému toku v nejcentrálnějších srážkách.

Ke studiju triangulárního toku ve srážkách Pb+Pb při težištové energii $\sqrt{s_{NN}} = 2.76$ TeV a ve srážkách Au+Au při $\sqrt{s_{NN}} = 200$ GeV byl použit Monte Carlo generátor HYDJET++, kombinující dvě nezávislé komponenty - "měkkou" část, založenou na parametrizaci relativistické hydrodynamiky, a "tvrdou" část řídící jety. Kombinací obou komponent lze získat realistické předpovědi toku pro značný počet různých hadronů. Model také umožňuje studium vlivu rozpadů částic na pozorovaný tok. Uskutečněné výpočty prokázaly, že distribuce triangulárního toku získané pomocí HYDJET++ jsou konzistentní s pozorovanými daty z LHC. Bohužel, při výpočtech pro RHIC nesouhlasí vypočítané hodnoty s hodnotami pozorovanými. Dále z našich výpočtů vyplývá, že rozpady těžkých rezonancí zvyšují maximální amplitudu pozorovaných distribucí triangulárního toku a posouvají maximum distribuce k vyšším příčným hybnostem. Rezonance, přesněji jejich rozpady, také velkou měrou přispívají ke splnění škálování toku počtem konstituentních kvarků daného hadronu. Jety naopak toto škálování, v případě LHC, narušují. Podobný efekt není patrný při srážkách na RHICu, jelikož v takto vzniklých systémech jsou jety výrazně méně energetické.

Klíčová slova: srážky těžkých jader, QGP, kolektivní pohyb, anisotropický tok, triangulární tok, LHC, RHIC, HYDJET++

Acknowledgement

Contents

List of Figures

List of Tables

Preface

Relativistic heavy-ion collisions provide a unique tool to study nuclear matter at extreme conditions, similar to those that prevailed in Early Universe shortly after Big Bang. A new state of matter – the quark-gluon plasma (QGP) – is predicted to be recreated at such high energy densities and temperatures. The QGP is a phase of deconfined quarks and gluons that behave asymptotically freely. The plasma created soon after the collision is very short-lived. In order of $10 - 30$ fm/c, the matter reaches the detector. By that time the quarks and gluons are yet again re-confined into hadrons which we can measure. As QGP cannot be observed directly, number of possible signatures were suggested: jet quenching, collective flow, suppression of heavy-flavoured hadrons etc.

The pressure gradients inside the system create an outward motion of particles - flow - which can be measured. The collective behaviour can yield information about bulk properties of the matter created in the collision. Two types of flow are distinguished - isotropic and anisotropic. The isotropic flow is generally manifested by additional boost in momentum of produced particles. The anisotropic flow originates from the initial asymmetry of the collision and manifests in x-y anisotropy. The system subsequently evolves as to reduce this spatial asymmetry, giving rise to momentum anisotropy. It is therefore a self-quenching phenomenon as once the fireball is spatially symmetric, the process stops. The expansion ceases at ~ 5 fm/c, any other modification of flow are due to interaction with the medium produced in the collision. Focusing on anisotropic flow, one can acquire information about the early stages of the collision and properties of the initial QGP state.

The azimuthal distribution of particles produced in relativistic heavy-ion collision can be expressed in a form of a Fourier series. The coefficients of the expansion v_n can be measured experimentally. Their values can yield information about the state of matter created in the collision. However, the magnitude of the flow coefficients decreases with their order. Originally, mostly the elliptic flow v_2 was investigated in heavy-ion experiments as the dominant component of anisotropic flow. With experiments reaching higher multiplicities and collecting more data, higher flow coefficients grow significantly in importance. Higher harmonics are necessary to correctly describe the geometry of the collision and the thermodynamical properties of created matter. Higher harmonics can also provide explanation for observed structures in two-particle correlation distributions.

The triangular flow is particularly interesting. The triangular flow v_3 originates from event-by-event fluctuations of the initial state. The corresponding anisotropy of the overlap region is referred to as triangularity. Unlike in the case of elliptic flow, the magnitude of

triangular flow does not depend on collision centrality. It has been suggested among other that the triangular flow v_3 can become the dominant component with certain initial conditions. It was recently confirmed that the elliptic and triangular flow are uncorrelated. It is essential to determine these two coefficients as the higher flow coefficients such as v_4, v_5 or v_6 can be to large extent reconstructed from v_2 and v_3.

While studying the flow of the most abundant hadrons, one needs to keep in mind that at high energies, most of those particles are produced via decay of hadron resonances. Such feed-down may greatly influence the observed flow. However, a significant part of the hadrons is produced from hghly collimated showers of particles nown as jets. Those are suspected to be the reason for observed number-of-constituent-quark scaling which is broken at LHC energies. Compared to RHIC, where the scaling holds true, LHC reaches much higher energies which result in more abundant and more energetic jets. Similar effects are also expected in the case of triangular flow.

Aim of our project is to simulate collective behaviour in relativistic heavy-ion collisions of lead ions at LHC and gold ions at RHIC. Main focus will be on triangular flow. Part of our study will focus how it is affected by decays of resonances. The study will be performed using the HYDJET++ Monte Carlo generator on UiO Abel cluster. HYDJET++ combines both soft hydro- and hard jet-part and is very well suited for collisions of heavy-ions ($A \geq 40$) at RHIC and LHC energies, $\sqrt{s_{NN}} = 200$ GeV and $\sqrt{s_{NN}} = 2750$ GeV respectively. The model is very efficient and is able to reproduce the interplay between the soft and the hard region. The model operates with a vast table of hadron resonances and the decays can be easily switched on or off, thus making the study of effects of heavy-resonance decay on flow coefficients feasible.

Chapter 1

Relativistic heavy-ion collisions and the quark-gluon plasma

Ultrarelativistic heavy-ion collisions represent a unique tool to probe matter at extreme conditions similar to the premordial Universe. At such extreme energy densities and temperatures, hadronic matter undergoes a phase transition into a state called quark-gluon plasma (QGP). The QGP is a state of asymptotically free quarks and gluons, which are normally confined within hadrons. Hence collisions of heavy-ion permit us to study the nature of this transition as well as properties of the strong interaction.

Figure 1.1 shows different phases of QCD matter at given baryon chemical potential μ_B (horizontal axis) and temperature T (vertical axis). μ_B is related to the net baryon density. During the Big Bang, equal amounts of matter and antimatter were produced and hence $\mu_B = 0$ for early Universe. Nowadays, we observe an abundance of matter over antimatter, corresponding to $\mu_B > 0$.

There are several ways the plasma can change back into hadrons. It can either experience a phase transition of nth order, which is manifested in discontinuity of nth derivatives of free energy F, or it can go through the so-called cross-over with no discontinuous derivative. Different transition scenarios are also depicted in Fig. 1.1 Current experiments at the RHIC and at the LHC observe matter at $\mu_B \sim 0$. According to QCD lattice calculations, the QGP created at such conditions should then cross over into hadronic gas at critical temperature $T_C \approx 170$ MeV. With increasing μ_B, the nature of the transition is expected to change into a first-order transition at the critical point. The RHIC Beam Energy Scan (BES) aims to investigate this problem in more details [2].

1.1 Hydrodynamical evolution of nucleus-nucleus collision

A schematic picture of a relativistic heavy-ion collision is shown in Fig. 1.2. The two nuclei collide at $t = 0$. After a brief and very dense pre-equilibrium stage, the plasma is formed
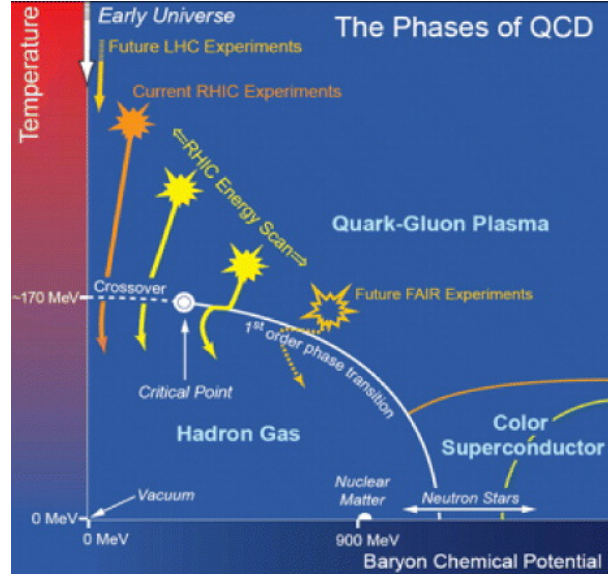
Figure 1.1: The QCD phase diagram. Taken from [1].

at $\tau_0 \sim 1$ fm/c after the collision. The system then starts to expand and cool down. Once the matter cools to critical temperature T_c, it experiences a gradual phase transition from QGP into hadronic gas. The system still evolves until it is fully hadronised - the medium reaches chemical freeze-out characterised by T_{ch}. The multiplicities of individual hadron species are fixed and do not change any further. However, the particles still interact one with each other through elastic scattering. At thermal freeze-out temperature T_{fo}, hadrons cease to interact and their thermal spectra are fixed.

The dense QGP stage can be described using hydrodynamical approach [5]. The originally predicted plasma was expected to behave as an ideal gas, i. e. with zero shear $\eta/s = 0$ and bulk viscosity $\zeta/s = 0$. Theoretical calculations have established a lower limit on shear viscosity [5]

$$\eta/s \gtrsim 1/4\pi. \tag{1.1}$$

Comparison of theoretical predictions with RHIC data for elliptic flow v_2 have yielded [6]

$$0.06 < \eta/s < 1.6. \tag{1.2}$$

Non-zero shear viscosity suggests strong coupling between individual matter consistituents. This validates macroscopical approach - rather than many individual little pieces, the bulk behaves as one object. As the discovered medium is not exactly the one predicted as the QGP, the term 'strongly-interacting quark-gluon plasma' (sQGP) may be sometimes used instead.

Naturally the idea of using hydrodynamics in description of a collision of heavy nuclei was tested via several observables [4]. One of them was number density n_i of particle
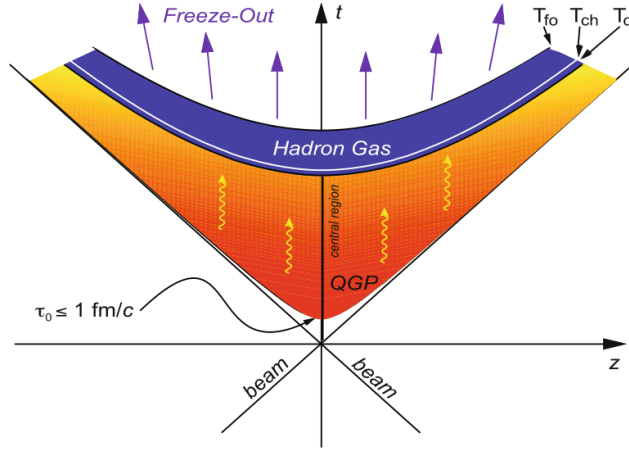
Figure 1.2: Space-time evolution of a collision of relativistic heavy ions. The horizontal axis denotes beam direction, the vertical axis represents time. The hyperbolas show proper time $\tau = \sqrt{t^2 - z^2}$. Taken from [3].

species i given as

$$n_i(T, \mu) = \frac{g}{2\pi} \int\limits_0^\infty \frac{p^2 \mathrm{d}p}{\exp\left(\frac{E_i - \mu_i}{T}\right) \pm 1}, \tag{1.3}$$

where T and μ denote temperature and baryon potential respectively, g stands for particle degeneracy factor, p denotes particle momentum and E its energy. The average number of given species $\langle N_i \rangle$ is fixed at the freeze-out, described by T_{fo} and μ_{fo}. The average number of particles is then obtained summing particles directly emitted (with number density n_i^{dir}) from the system of volume V and those coming from decays of resonances (number density n_R):

$$\langle N_i \rangle = V \left(n_i^{dir}(T, \mu) + \sum \Gamma(R \to i) n_R(T, \mu) \right), \tag{1.4}$$

where $\Gamma(R \to i)$ is the branching ratio of considered channel.

Ratios of various species are shown in Fig. 1.3. Then the size of the system represented by V is cancelled out and the ratio is a function of T and μ only. One can see that fitting the data with ratios of species numbers given by 1.4 works remarkably well.

1.2   Experimental observables and signatures of the QGP

Due to the very short lifetime of the QGP phase, it cannot be observed directly. Only the hadrons in the final state can be measured. Several observables are considered as signatures of the QGP. In the following text, we will discus some of them.
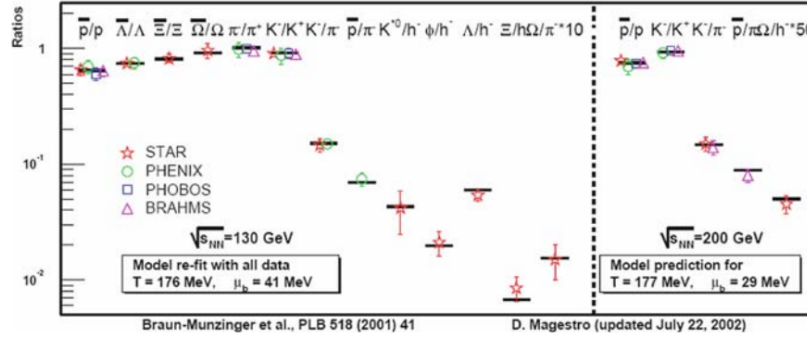
Figure 1.3: Particle ratios at the RHIC. Taken from [4].

Collective flow

Collectivity of the created matter suggests thermalisation of the medium. Thorough description is given in Sec. 1.3.

Suppresion of nuclear modification factor R_{AA}

To show how much the production of various particles is affected by the medium, the nuclear modification factor R_{AA} is used. R_{AA} is defined as a ratio of particle yield in A+A collision to the yield in p+p collision normalised by the average number of binary collisions per event $\langle N_{bin} \rangle$,

$$R_{AA} = \frac{1}{\langle N_{bin} \rangle} \frac{\mathrm{d}^2 N_{AA}(p_T)/\mathrm{d}p_T \mathrm{d}y}{\mathrm{d}^2 N_{pp}(p_T)/\mathrm{d}p_T \mathrm{d}y}. \tag{1.5}$$

If the nuclear modification factor is equal to unity, $R_{AA} = 1$, no medium effects are observed. In central A+A collisions at maximum energy at RHIC and at LHC, R_{AA} is much less than 1. Fig. 1.4 shows suppression of light hadrons and non-prompt J/Ψ in CMS data [8]. Both are visibly bellow 1. On the other hand, measurements of electroweak probes (γ, W and Z^0) show no suppression. This is expected as such particles should not interact with the plasma and should thus remain unaffected by the medium, in contrast to the hadrons.

In what concerns heavy quarks, both charm and beauty quarkonia and open-charm hadrons can be studied. Heavy quarks are produced in the early stages of the collision, during the initial hard scattering processes. They interact with the medium and the resulting modification of their properties can therefore unveil new information about the medium. In the deconfined medium, the presence of free colour charge is expected to screen the binding potential between the quark-antiquark pair. The larger the system is, the less it is bound and therefore breaks-off due to the colour screening more easily. Excited quarkonia systems are of larger size and weaker binding energy. Hence the spectral
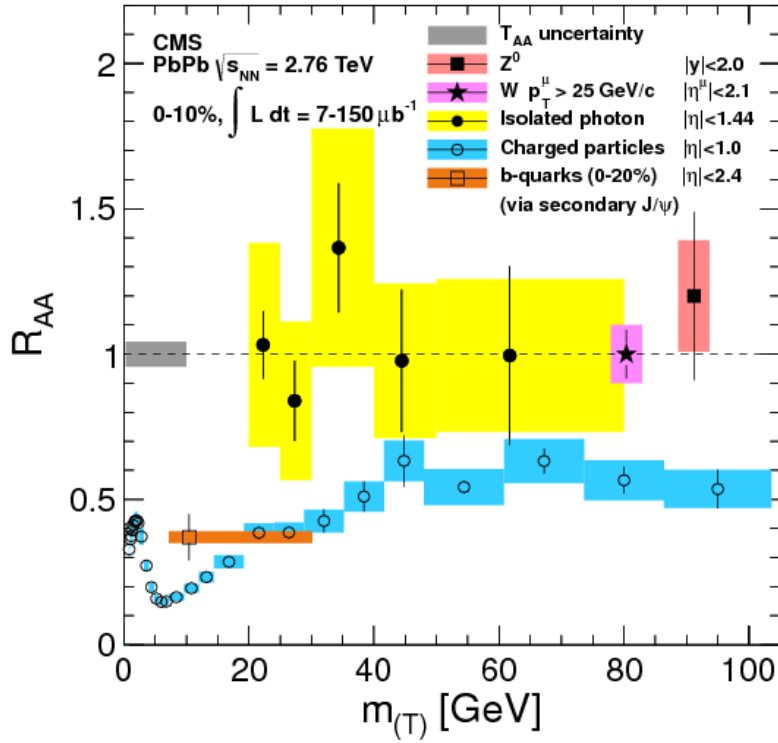
Figure 1.4: Nuclear modification factor R_{AA} as a function of transverse mass m_T. Shown are $R_{A}A$ for light hadrons (blue open circles), non-prompt J/Ψ (brown open square), photons (yellow full circles), W and Z^0 (violet star and full red square respectively). Taken from [8].

analysis of heavy-flavoured quarkonia could provide a QGP thermometer provided all other effects that influence the spectrum would be understood.

The R_{AA} for heavy hadrons was predicted to be higher than for light hadrons due to smaller energy loss, but experimental observation revealed that the suppression for both kinds is about the same [9].

Suppresion of high-p_T particles

Jets are highly collimated showers of partons originating from high-energy parton scattering, which occur during the initial stage of the collision. The two partons that were initially scattered then travel in opposite directions. Should the scattering take place close to the surface of the fireball, one parton would then quickly leave the medium while the other one would have to travel through the formed plasma. The jet travelling through the hot matter would experience many collisions with the partons in the medium and would

loose much more energy compared to the other jet. Such a phenomenon is refered to as jet quenching.
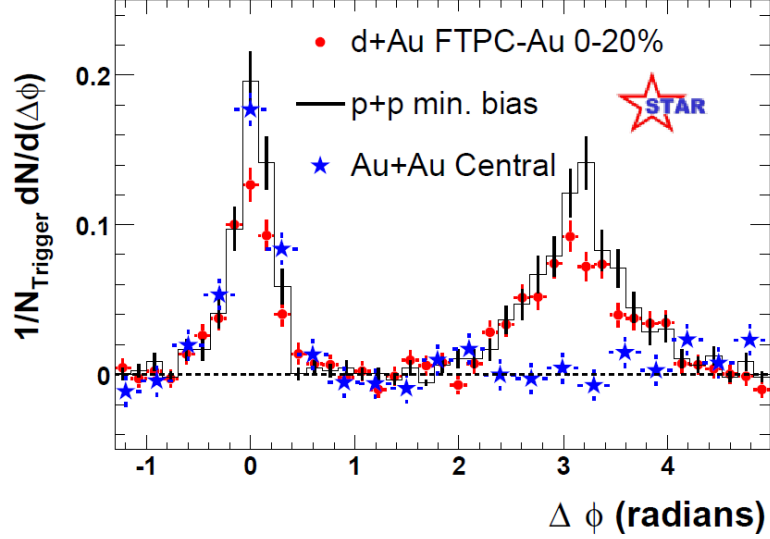
Figure 1.5: Distribution of associated particles with respect to the trigger particle (at $\Delta\phi = 0$) for p+p, d+Au and Au+Au at $\sqrt{s_{NN}} = 200$ GeV performed by STAR. The near-side jet ($\Delta\phi = 0$) is present for all systems. The away-side jet ($\Delta\phi = \pi$) is visible for p+p and d+Au only. Therefore we conclude that the away-side jet was absorbed while traversing the QGP. Taken from [10].

Figure 1.5 shows the azimuthal angular correlation function between the trigger particle, fullfiling $4 < p_T(trig) < 6$ GeV/c, and associated particles with lower momentum ($2 < p_T(assoc) < pt(trig)$) for p+p, d+Au and Au+Au at $\sqrt{s_{NN}} = 200$ GeV [10]. Two peaks are clearly visible in p+p and d+Au collisions, one at $\Delta\phi = 0$ (near-side jet) and the other one at $\Delta\phi = \pi$ (away-side jet). No QGP is expected to form in these systems. However, in Au+Au collisions, the away-side jet vanishes. The explanation is that the jet undergoes many collisions with the partons inside the hot and dense matter and therefore looses most of its energy.

Electromagnetic probes

The matter created in collisions of heavy ion can be also probed using electromagnetic signatures, i. e. thermal photons and dileptons [11]. Both have large free mean path, meaning they are very unlikely to interact with the medium. Instead, they will travel directly into detector.

Dileptons can be formed in QGP through the annihilation of quark pair

$$q + \bar{q} \longrightarrow l^+ + l^-. \tag{1.6}$$

The dilepton distribution would then vary about the same as the initial quark distribution, meaning that the dilepton temperature is approximately the same as the temperature of the original $q\bar{q}$ pair and hence of the medium. Thus by measuring the thermal distribution of dileptons created in collisions of heavy nuclei one can extract the temperature of the fireball during the time of the l^+l^- pair creation. The measurement is however affected by a vast number of competing processes, including dileptons created in Drell-Yan process or in decays of hadrons and resonances. So far, no conclusive answer on QGP from dilepton measurements has been provided [12, 13].

Photons can be formed from the QGP as

$$q + \bar{q} \longrightarrow \gamma + g \tag{1.7}$$

either through $q\bar{q}$ annihilation or through Compton scattering. As in the previous case, this would grant direct access to the thermodynamics of the medium at the very moment of the production of the detected photon and hence the immediate temperature of the QGP phase. In PHENIX [13], the average temperature of the medium is

$$T = 221 \pm 19_{(stat)} \pm 19_{(sys)} \text{ MeV}, \tag{1.8}$$

while in ALICE [14], shown in Fig. 1.6,

$$T = 304 \pm 51_{(sys+stat)} \text{ MeV}. \tag{1.9}$$
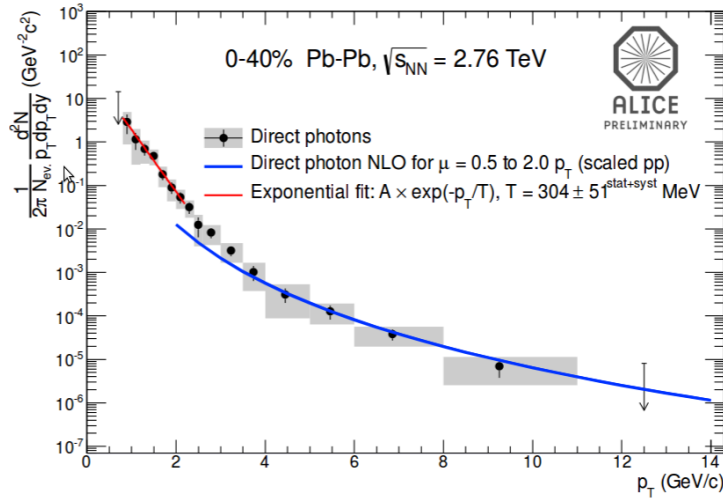
Figure 1.6: Direct photon spectrum in Pb+Pb at $\sqrt{s_{NN}} = 2.65$ TeV (points) and in *pp* collisions (solid blue line) at ALICE. Red line represents thermal fit to the data. Taken from [14].

1.3 Collective flow of particles

As the medium thermalises through secondary collisions of the constituents, pressure develops in the system. The pressure gradients inside the fireball create an outward motion of the matter. The invariant differential cross section of the particle reaching the detector can be expanded into a Fourier series w. r. t. reaction plane Ψ_R:

$$E\frac{\mathrm{d}^3N}{\mathrm{d}^3p} = \frac{1}{2\pi}\frac{\mathrm{d}^2N}{p_T\mathrm{d}p_T\mathrm{d}y}\left(1 + \sum_{n=1}^{\infty} 2v_n \cos\left(n\varphi - n\Psi_R\right)\right) \tag{1.10}$$

$$v_n = \langle\cos\left(n\varphi - n\Psi_R\right)\rangle$$

where p_T stands for transverse momentum, y denotes rapidity and φ represents azimuthal angle of the particle [15]. Ψ_R is defined by b and beam direction z.
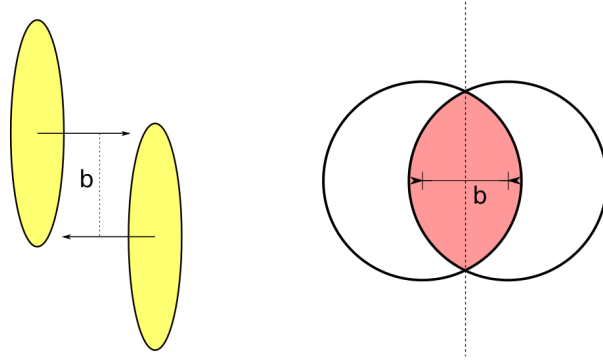
Figure 1.7: Schema of a peripheral heavy-ion collision. The two nuclei collide with impact parameter b. The overlap region is asymmetric and can be expressed as a function of b.

The first term in brackets represents isotropic flow, in other words the isotropic expansion of the fireball. Isotropic flow gives additional boost to the particles, manifested as a low-p_T 'shoulder-structure' in hadron transverse momentum spectra [4]. Anisotropic flow, denoted by the sum in Eq. 1.10, describes anisotropy of the initial overlap zone. In a peripheral collisions such as shown in Fig. 1.7, the two nuclei collide with a non-zero value of the impact parameter b, resulting in an elliptically shaped overlap zone. As the fireball evolves, spatial anisotropy decreases, giving rise to momentum anisotropy. A simple explanation of the situation is illustrated in Fig. 1.8a. The strongest pressure gradient in the originally almond-shaped fireball is along the direction with least matter in the way. Most matter will move in this direction due to least resistance from the medium and will gain most momentum. Particles moving perpendicular to this direction will struggle more to exit the zone, gaining significantly less momentum.
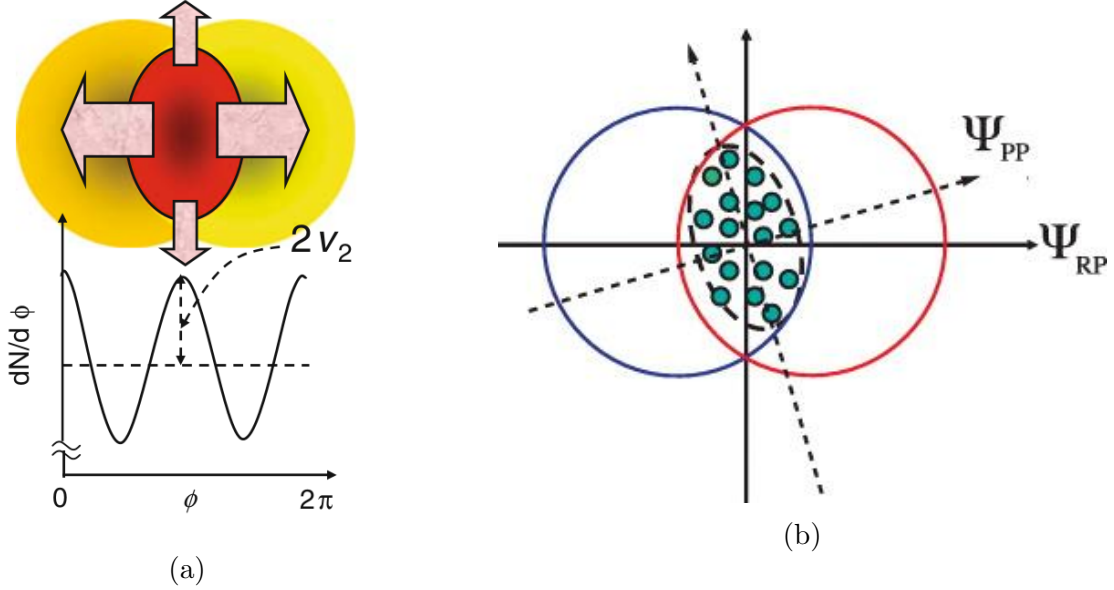
Figure 1.8: (a) Pressure gradients in the fireball and azimuthal distribution $dN/d\phi$ in a peripheral heavy-ion collision. Taken from [4]. (b) Reaction plane Ψ_R versus participant plane Ψ_{PP}. The dashed ellipse shows the actual overlap zone, the geometrical zone is defined as the intersection of the two nuclei. Taken from [16].

1.3.1   Elliptic flow

Elliptic flow has been measured over a wide range of collision energies as shown in Fig. 1.9a. While at lower centre-of-mass energies per nucleon pair $\sqrt{s_{NN}}$ the elliptic flow changes rather drastically, for $\sqrt{s_{NN}} \gtrsim 5$ GeV it increases logarithmically [19].

The magnitude of elliptic flow depends on medium properties, e. g. shear viscosity η/s, and on initial spatial anisotropy as

$$v_2 \propto \frac{\langle y^2 + x^2 \rangle}{\langle y^2 - x^2 \rangle} \tag{1.11}$$

The sign of v_2 signifies the preferential region of expansion: in-plane for $v_2 > 0$ and out-of-plane if $v_2 < 0$. The sign change can be explained as follows:

- $v_2 > 0$ at low $\sqrt{s_{NN}}$: a rotating nucleus is formed, which subsequently decays with fragments flowing in the reaction plane;

- $v_2 < 0$: expansion of produced matter is hindered by spectators in the reaction plane, the matter is then squeezed out of the reaction plane;

- $v_2 > 0$: with growing energy, spectators leave the reaction zone which allows the matter to expand in reaction plane.
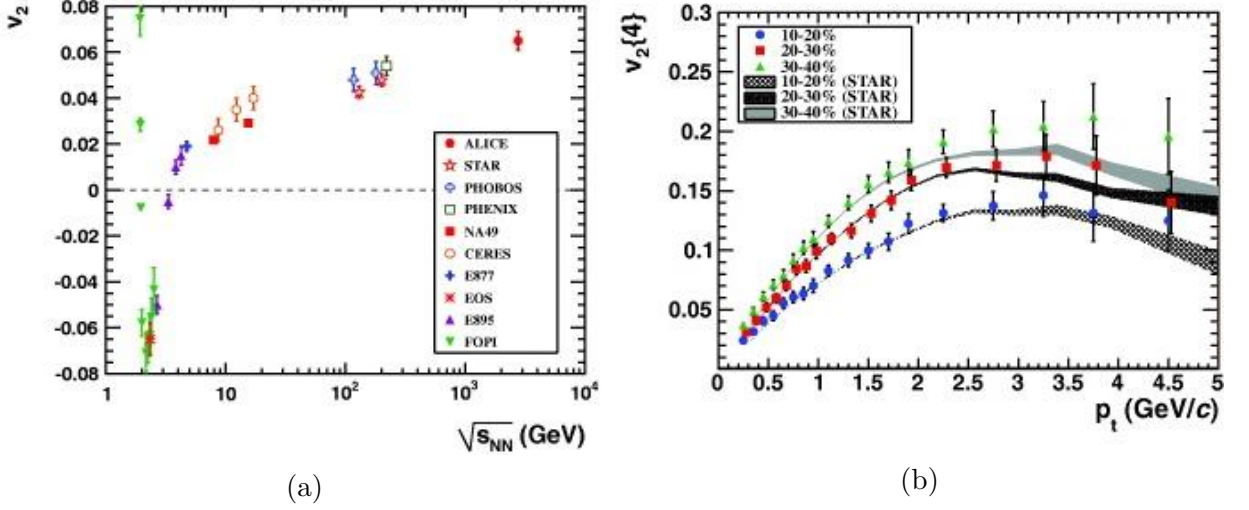
Figure 1.9: (a) Integrated elliptic flow at different centre-of-mass energies. (b) Comparison of $v_2(p_T)$ in ALICE data (points) with STAR measurements (bands). Both taken from [18].

Comparison between RHIC and LHC data is shown in Fig. 1.9b. The plot shows elliptic flow as a function of p_T. LHC data are denoted by data points while RHIC data are shown as bands. Hydrodynamical calculations predict similar character of the medium observed at ALICE and at STAR.

At low transverse momenta, lighter hadrons usually carry stronger elliptic flow than heavier ones. This phenomenon is known as mass ordering and originates in the interplay between radial and anisotropic flow. An example can be found in Fig. 1.10. At fixed p_T up to $\gtrsim 1.5$ GeV/c,

$$v_2^\pi > v_2^K > v_2^p > v_2^{\Lambda+\Xi}.$$

Above the threshold p_T, the mass ordering is broken, with heavier baryons carrying stronger flow.

A very interesting feature, first observed by PHENIX in 2008 [22], is the number-of-constituent-quark scaling of the elliptic flow. Fig. 1.11a shows the scaled v_2 distributions of identified particles at RHIC. In the left plot, p_T dependence of v_2 was simply modified to show $v_2/n_q(p_T/n_q)$. However, it is better to plot elliptic flow as a function of transverse kinetic energy defined as

$$kE_T = \sqrt{p_T^2 + m^2} - m, \tag{1.12}$$

where m is the rest mass of a given hadron species. Then it is easy to see that for each species, $v_2/n_q(kE_T/n_q)$ up to $kE_T \approx 1.5$ GeV is the same. This phenomenon can be explained by early development of the flow, still during parton phase rather than during hadron phase. Each quark then carries the same flow and for the whole hadron

$$v_2^{\text{hadron}}(kE_T/n_q) \approx n_q v_2^{\text{quark}}(kE_T/n_q). \tag{1.13}$$
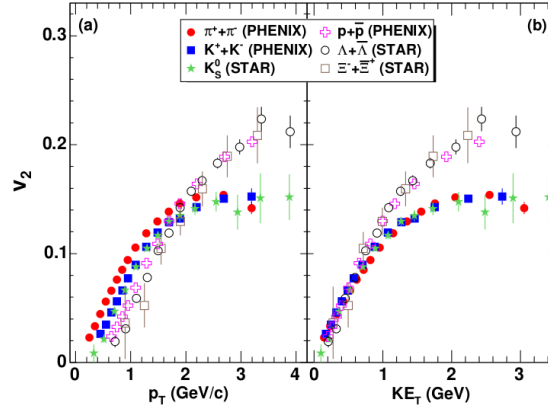
Figure 1.10: Elliptic flow v_2 as a function of p_T of identified hadrons. Taken from [22].

Similar measurement from ALICE in Pb+Pb at $\sqrt{s_{NN}} = 2.76$ TeV can be found in Fig. 1.11b. One does immediately spot that scaling is broken at LHC energies. This can be attributed to jets which are more energetic and much more abundant at the LHC than at the RHIC [38].

(a)   (b)
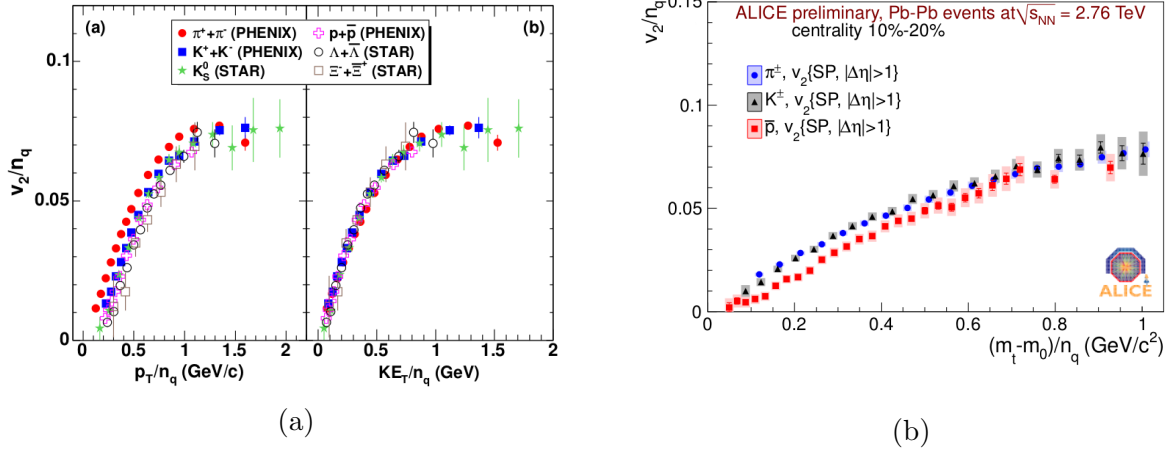
Figure 1.11: (a) $v_2/n_q(p_T/n_q)$ (left) and $v_2/n_q(kE_T/n_q)$ (right) for identified particles in minimum-bias Au+Au collisions at $\sqrt{s_{NN}} = 200$ GeV at RHIC. Taken from [22]. (b) $v_2/n_q(kE_T/n_q)$ for identified particles at $\sqrt{s_{NN}} = 2.76$ TeV in ALICE experiment. Taken from [24].

1.3.2   Triangular flow

The spatial anisotropy gives rise to even harmonics such as v_2. The odd harmonics are on the other hand created in the fluctuations of the overlap zone and vanish in the event

average, e. g in the case of the triangular flow

$$\langle v_3(\Psi_R) \rangle = 0. \tag{1.14}$$

Hence to study the triangular flow and higher odd harmonics one needs to investigate event-by-event fluctuation in each collision. The situation is illustrated in Fig. 1.8b. The reaction plane $\Psi_R P$ defines a geometrical overlap zone at fixed centrality. However, the actual overlap zone, defined by participant plane Ψ_{PP}, fluctuates event by event around the average event plane.

Bearing this in mind, it is only natural to redefine the flow coefficients to describe single event rather than a whole set. Then

$$v_n(\Psi_n) = \langle \cos(n\varphi - n\Psi_n) \rangle, \tag{1.15}$$

where we define each coefficient w. r. t. the corresponding minor axis Ψ_n (see Fig. 1.12). Ψ_n defines the direction of the strongest pressure gradient relevant to the specified flow harmonic v_n.
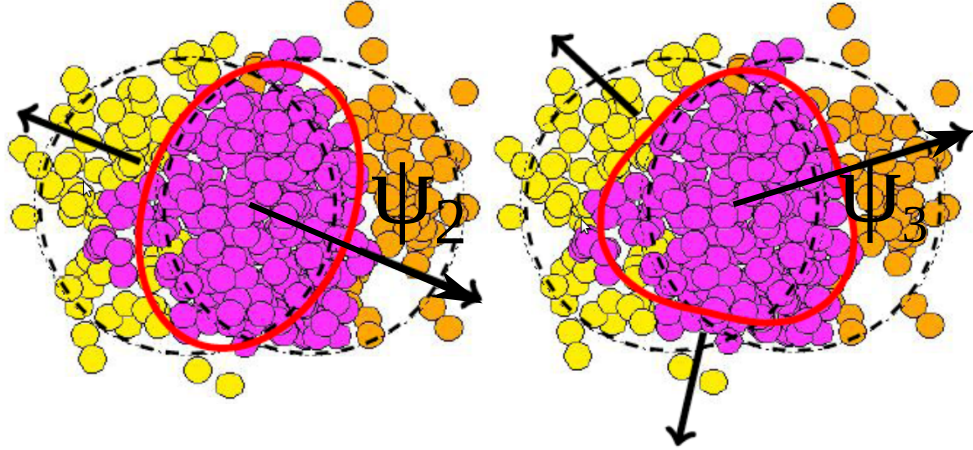
Figure 1.12: Event-by-event fluctuations of the overlap zone in a heavy-ion collision. Taken from [17].

Ψ_2 is generally assumed to coincide with the reaction plane Ψ_R, while Ψ_3 is uncorrelated with either, therefore

$$\langle v_3(\Psi_2) \rangle = 0. \tag{1.16}$$

Chapter 2

Recent experimental results

The elliptic flow has been studied excessively in different systems and at different energies. Since magnitude of the n$^{\text{th}}$ harmonic decreases with its order, flow coefficients of order $n \geq 3$ are significantly less pronounced. For instance, in 2004 STAR measured $v_6 = 0.043 \pm 0.037$ and $v_8 = -0.06 \pm 0.14$ which is consistent with zero [20]. Due to the much greater collision energies at the LHC than at any other other facility, the multiplicities in recorded events are significantly greater. Additionally, the fluctuations are also more crucial. Higher harmonics then grow in importance.

Experiments at the LHC have measured distributions for multiple flow coefficients (up to $n = 6$) [23, 26] in Pb+Pb collisions at $\sqrt{s_{NN}} = 2.76$ TeV over the pseudorapidity interval $|\eta| < 0.8$ for ALICE and CMS and over $|\eta| < 2.5$ at ATLAS. STAR has also recently released first results of the triangular hadronic flow.

In this chapter, we will briefly sum up the most interesting results.

2.1 Anisotropic flow at the LHC

ATLAS Collaboration recently released measurements of anisotropic flow distributions $v_n(p_T)$ up to $n = 6$. v_2–v_6 as a function of p_T for different centrality bins within the range of $0-30\%$ can be found in Fig. 2.1. In all centrality bins we see that indeed the magnitude of each harmonic decreases with its order. However in the most central events ($0 - 5\%$, upper left panel) v_3 outgrows v_2 while v_4 is as strong as v_2. The harmonic that contributes the most in the head-on events is thus v_3.

Figure 2.2 shows integrated flow coefficients v_n for $n = 2, 3, 4$ as a function of centrality in ALICE data [23]. The v_2 distribution (red circles) varies with centrality, reaching its maximum for peripheral collisions at $40 - 50\%$. The distributions of v_3 (denoted by open and full blue squares, depending on the applied method) and v_4 (pictured as magenta asterisks), on the other hand, show weak centrality dependence. The magnitude of observed triangular flow corresponds to low shear viscosity of the medium η/s, as generally assumed [23]. In addition, distributions of $v_3(\Psi_R)$ and $v_3^2(\Psi_2)$ are also plotted as green circles and black diamonds respectively. Both sets of data are consistent with zero
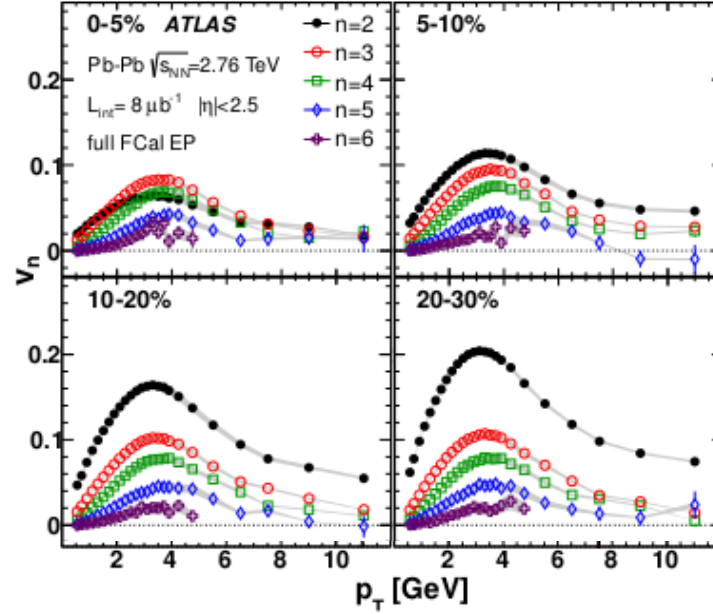
Figure 2.1: $v_n(p_T)$ for $n = 2 - 6$ in Pb+Pb collisions at the ATLAS experiment over centrality range $0 - 5\%$, $5 - 10\%$, $10 - 20\%$ and $20 - 30\%$. Taken from [26].

which agrees with Eq. 1.14 and Eq. 1.16.

Measurements of multiple flow coefficients also bring more insight into characteristics of the created hot and dense matter. The triangular flow is expected to be more sensitive to viscosity than the elliptic flow. Comparison of measured v_2 and v_3 with predictions for different viscosity scenarios was performed by ALICE, see Fig. 2.3. At low p_T, the $v_2(p_T)$ is well described by $\eta/s = 0$, the $v_3(p_T)$ corresponds better to the viscosity $\eta/s = 0.08$.

Interplay of higher flow coefficients may explain occurrence of specific structures in two-particle correlation, such as the peak on the near side and the ridge structure on the away-side. Both structures in Pb+Pb events are displayed in Fig. 2.4a. The ridge structure in particular was discussed to be the manifestation of triangular flow in the system [17]. Combination of harmonics v_2–v_6 naturally yields good prediction of the observed correlation structure, as shown in Fig. 2.4b.

To test the degree of plasma thermalisation and how strongly it is coupled, magnitudes of v_2 and v_4 and the ratio v_4/v_2^2 have been previously investigated in RHIC data [20, 27]. The ratio of $v_n^{1/n}/v_2^{1/2}$ for $n = 3, 4, 5, 6$ has been studied by ATLAS [26]. According to previous measurement of v_4/v_2^2 performed at STAR, the ratio is expected to be constant in p_T. Measured values of $v_n^{1/n}/v_2^{1/2}$ are shown in Fig. 2.5a. With the exception of the most central values (centrality range $0 - 5\%$) the data show weak or no p_r dependence, which agrees with ideal hydro. All distributions do however vary strongly with centrality, one can also mark a slight dependence on n. The centrality dependence can be better
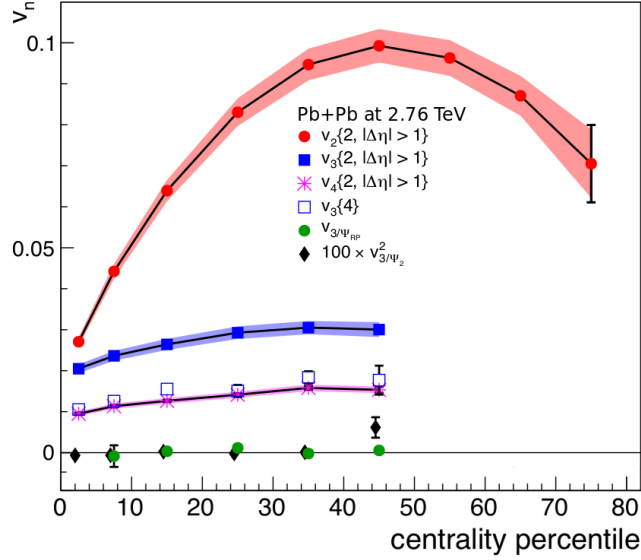
Figure 2.2: v_2 (red circles), v_3 (blue squares) and v_4 (magenta asterisks) versus event centrality in Pb+Pb collisions at $\sqrt{s_{NN}} = 2.76$ TeV, integrated over transverse momentum range $0.2 < p_T < 5.0$ GeV/c. Full and open squares denote different method of extracting v_3. Green circles represent $v_3(\Psi_R)$ while black diamonds show $v_3^2(\Psi_2)$. Taken from [23].

seen in Fig. 2.5b, displayed values of $v_n^{1/n}/v_2^{1/2}$ were integrated over transverse momentum (2 GeV/c < p_T < 3 GeV/c). In semi-peripheral and peripheral events, $\sim 20 - 60\%$, the ratios display weak centrality dependence. At centrality bellow 20%, $v_n^{1/n}/v_2^{1/2}$ increases rapidly. For $n = 4, 5, 6$, the distributions are nearly identical while $n = 3$ seems to differ slightly. Since previous plot proved weak p_T dependence, this is assumed to hold over the whole p_T range.

Number-of-constituent-quark scaling of the elliptic and the triangular flow of identified particles has been investigated by ALICE [24]. v_2/n_q shows breaking of transverse kinetic energy scaling kE_T/n_q, as discussed in Ssec. 1.3.1. The triangular flow as a function of p_T for pions, kaons and anti-protons is shown in Fig. 2.6a, the scaling v_3/n_q versus kE_T/n_q is shown in Fig. 2.6b .Qualitatively speaking, v_3 exhibits similar features to v_2, such as mass ordering, splitting of branches and as in case of $v_2/n_q(kE_T/n_q)$, the scaling is broken for $v_3/n_q(kE_T/n_q)$.

2.2   Anisotropic flow at the RHIC

STAR has recently released first results of anisotropic flow measurement [21] over a wide centre-of-mass energy range. $v_3(p_T)$ of identified hadrons in Au+Au at $\sqrt{s_{NN}} = 200$ GeV
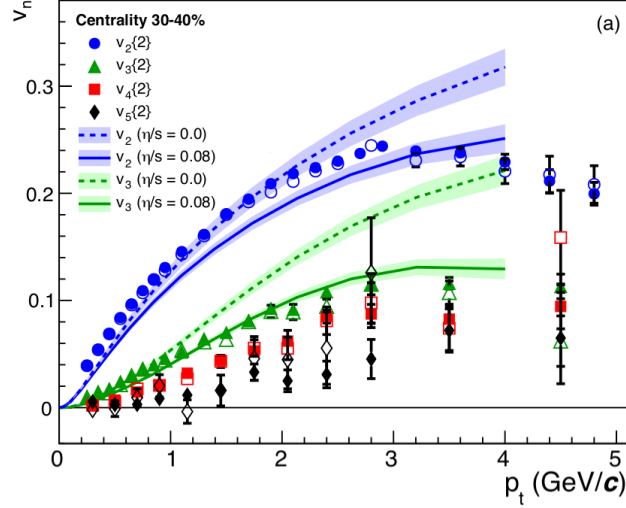
Figure 2.3: v_2 (blue circles), v_3 (green triangles), v_4 (red squares) and v_5 (black diamonds) as a function of p_T in Pb+Pb collisions at $\sqrt{s_{NN}} = 2.76$ TeV at centrality $30 - 40\%$. Full and open symbols represent data at $\Delta\eta > 0.2$ and at $\Delta\eta > 1.0$ respectively. Lines show hydrodynamic predictions for different viscosity scenarios. Taken from [23].

and 39 GeV are shown in Fig. 2.7. At 200 GeV, the v_3 distributions display clear mass ordering in the lower p_T region, while at 39 GeV the distributions are rather similar for all species. This suggest stronger radial flow at 200 GeV than at 39 GeV [28].

Two different scenarios for v_3 NCQ scaling were studied at STAR, see Fig. 2.8. The upper plots show the triangular flow in Au+Au collisions at 200 GeV and 39 GeV as a function of kE_T/n_q. The first scaling scenario, $v_3/n_q(kE_T/n_q)$ is shown in the two middle plots. Mesons seem to scale rather well but protons deviate significantly for both collisions energies. Model calculations suggest that $v_3/n_q^{3/2}(kE_T/n_q)$ should provide a better scaling picture [29]. This was also studied by STAR and the results can be seen at the bottom panel. At 200 GeV, the scaling is achieved. It is not so at 39 GeV, yet one can spot visible improvement.

In the upcoming Beam Energy Scan II programme, NCQ scaling will be studied in more detail [28].

2.3 Flow measurements in p-Pb collisions

Collisions of $p - A$ serve as a reference for AA collisions, to enable distinction between cold nuclear effects and true signs of QGP production. Long-range correlations of hadrons were measured at ALICE [30] in p+Pb collisions at $\sqrt{s_{NN}} = 5.02$ TeV. From those, Fourier coefficients were extracted. Fig. 2.9 shows measured v_2 for all and identified hadrons. The data were obtained from high-multiplicity events (20% of the most central events) from
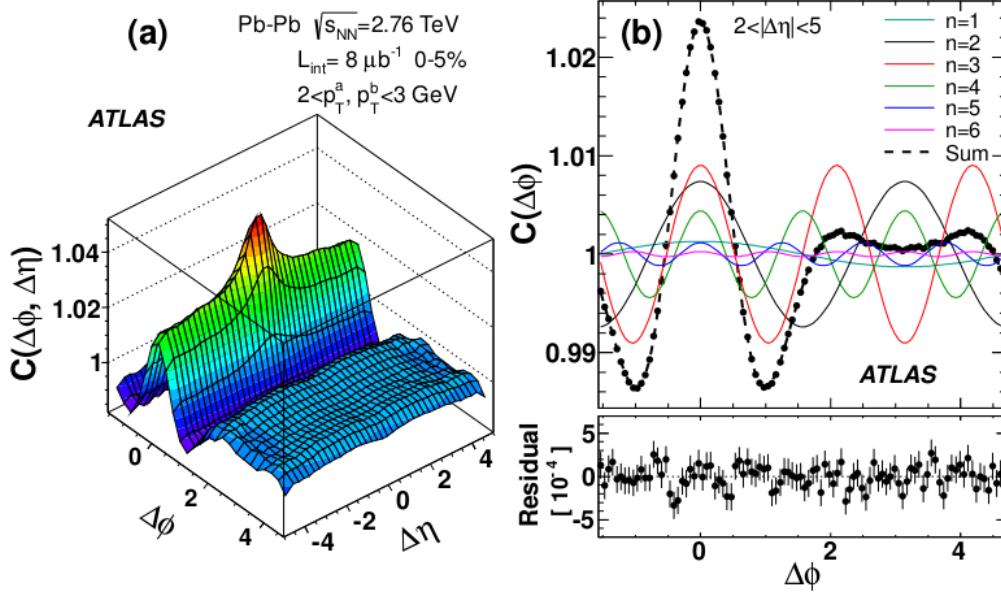
Figure 2.4: (a) The two-dimensional two-particle azimuthal correlation function at $0 < \phi < \pi$ and at $|\eta| < 5$, measured in Pb+Pb at $\sqrt{s_{NN}} = 2.76$ TeV. (b) The two-particle azimuthal correlation function in azimuthal range $0 < \phi < \pi$. Solid lines represent v_n for $n = 2, 3, 4, 5, 6$. Dashed line shows their sum. Taken from [26].

which low-multiplicity, peripheral, events were subtracted to reduce effects arising due to jets.

Resulting v_2 looks qualitatively the same as in AA collisions, see for instance Fig. 1.10. The distribution of identified particles bear hints of mass ordering, as at fixed $p_T < 2$ GeV/c

$$v_2^p < v_2^K \lesssim v_2^\pi. \tag{2.1}$$

At $p_T \approx 2$ GeV/c, crossing of the meson and baryon branches occurs.

This is very intriguing indeed as such behaviour was originally unexpected. Collisions of $d + Au$ at the RHIC have also revealed similar behaviour at lower energies. Explanation of this phenomenon is awaited.

(a) (b)
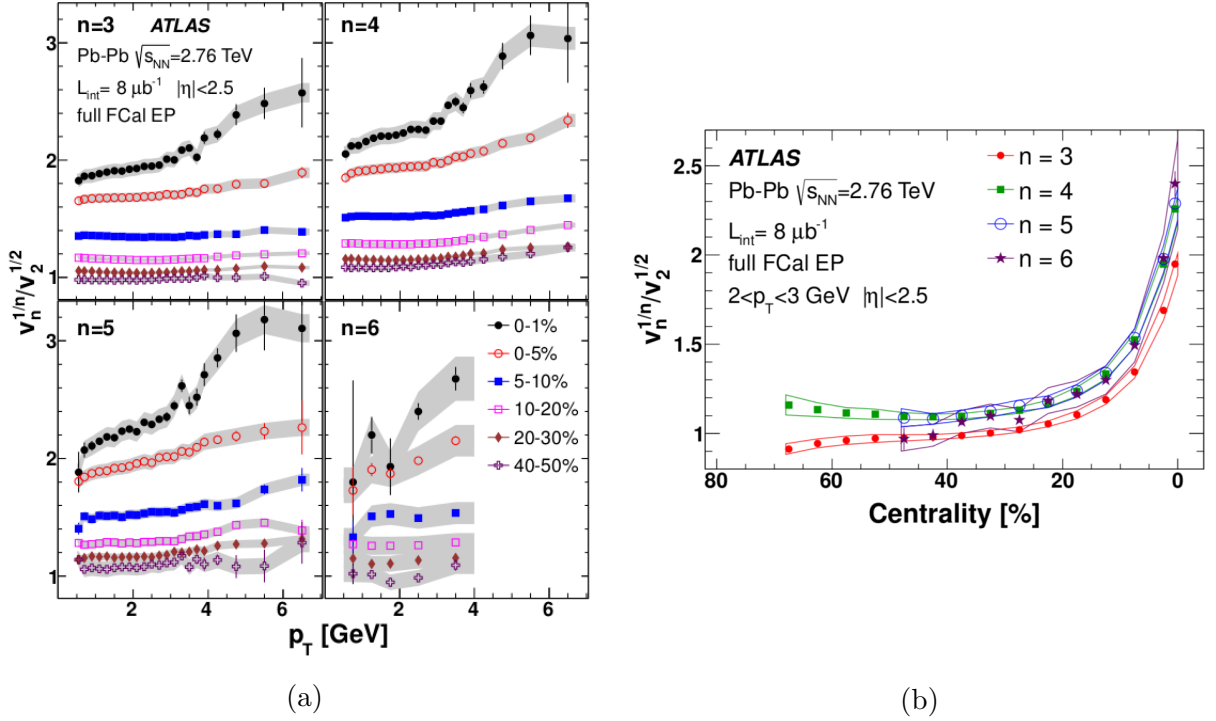
Figure 2.5: (a) The ratio $v_n^{1/n}/v_2^{1/2}$ for $n = 3, 4, 5, 6$ as a function of p_T for several centrality intervals. (b) $v_n^{1/n}/v_2^{1/2}$ versus centrality. Taken from [24].

(a) (b)
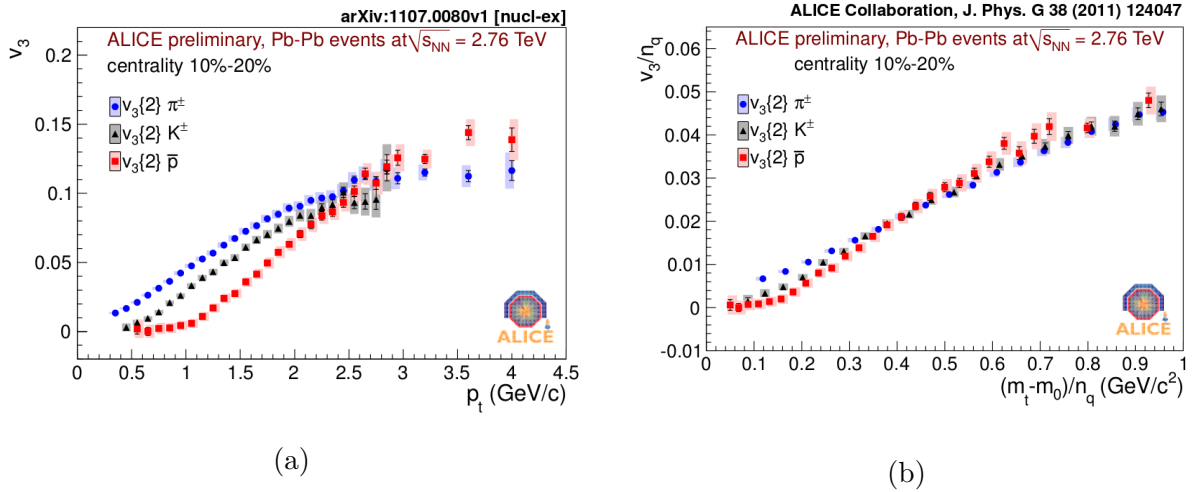
Figure 2.6: (a) $v_3(p_T)$ of identified hadrons in Pb+Pb at $\sqrt{s_{NN}} = 2.76$ TeV at $10 - 20\%$ centrality window. (b) v_3/n_q distribution as a function of kE_T/n_q in the same dataset. Both taken from [24].
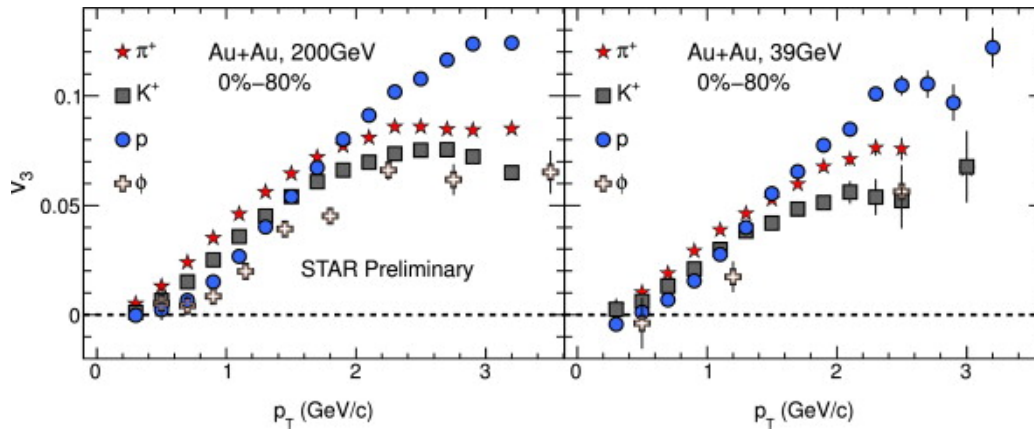
Figure 2.7: $v_3(p_T)$ of identified hadrons in (a) Au+Au at $\sqrt{s_{NN}} = 200$ GeV and in (b) Au+Au at $\sqrt{s_{NN}} = 39$ GeV. Taken from [28].
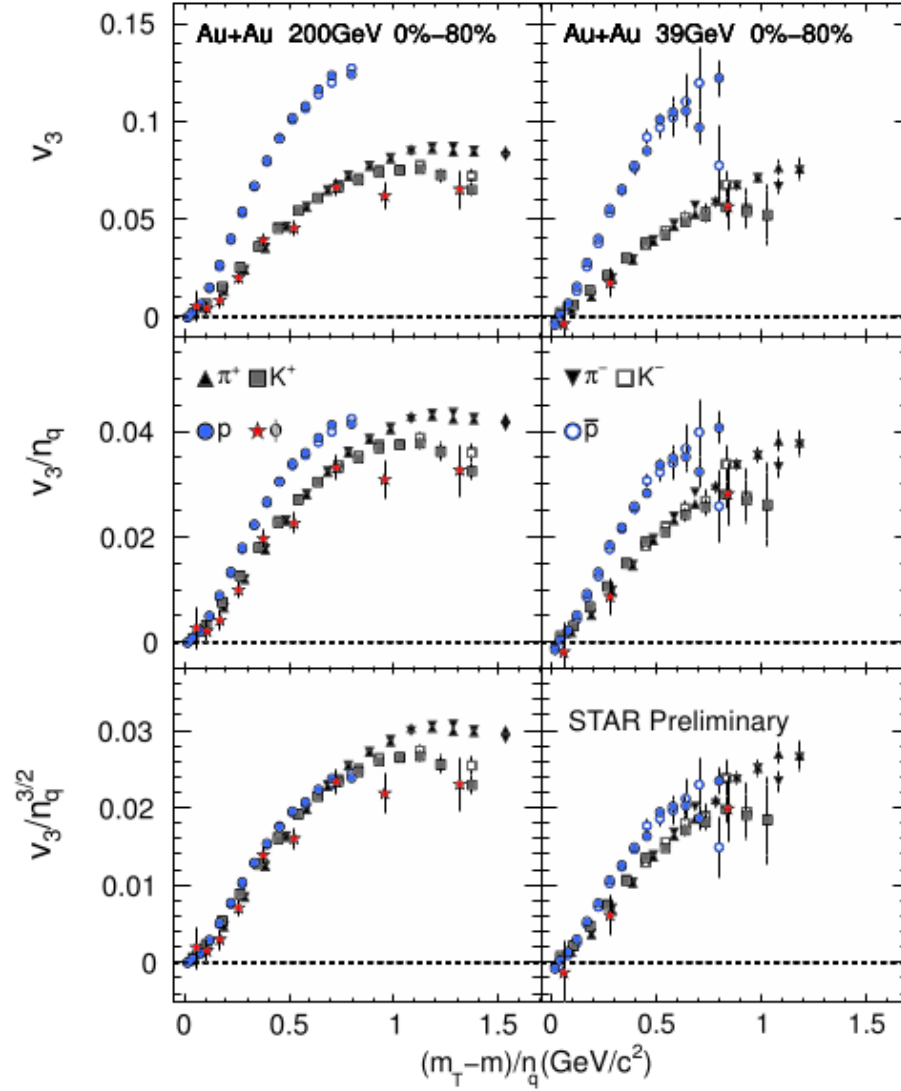
Figure 2.8: Number-of-constituent-quarks scaling for v_3 of identified particles for minimum bias Au+Au collisions at $\sqrt{s_{NN}} = 200$ GeV (left) and $\sqrt{s_{NN}} = 39$ GeV (right). *Upper panels* show $v_3(kE_T/n_q)$, *middle panels* display $v_3/n_q(kE_T/n_q)$ and finally in *bottom panels* the $v_3/n_q^{3/2}(kE_T/n_q)$ can be found. Taken from [28].
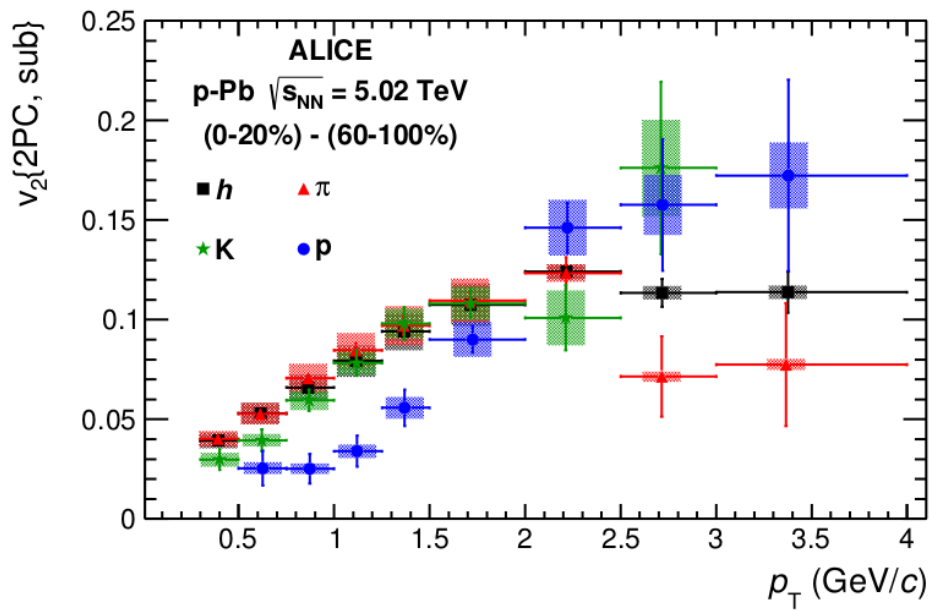
Figure 2.9: Second Fourier coefficient v_2 as a function of p_T for all hadrons (black squares), pions (red triangles), kaons (green stars) and protons (blue circles). Taken from [30].

Chapter 3

HYDJET++

In this chapter, we will briefly describe the hardware and software used during our study. Calculations were done running HYDJET++ , which is described in Sec. 3.1, at Abel [31]. Abel is a computer cluster at the University of Oslo, composed of over 650 nodes and more than 10000 cores. Effective usage of the Abel infrastructure is ensured by the Slurm queue system.

3.1   Description of HYDJET++

HYDJET++ is a Monte Carlo heavy-ion event generator [32], mostly written in C++ with a dash of FORTRAN. Installation package is available on the internet and free to use [33]. The model was designed for wide range of heavy-ion experiments ($A \gtrsim 40$). It was optimised and tested for RHIC (previous versions, only containing v_2) and for LHC (current[1] version 2.2, including v_3).

HYDJET++ is a superposition of a soft hydrodynamical part and a hard part containing jets. The two parts are treated independently. The soft part generates hadrons on a hypersurface described by a parametrisation of relativistic hydrodynamics at given initial conditions and equation of state. The hard part is based on PYQUEN and deals with binary collisions at given impact parameter b. Resulting partons with transverse momentum exceeding threshold value p_T^{min} are further evolved, experiencing radiative and collisional losses in the medium. Partons with $p_T < p_T^{min}$ are thermalised, their hadronisation products being included in the soft component. p_T^{min} is a model parameter and its value can be modified by the user. HYDJET++ comes with a pre-set value of this parameter for both LHC and RHIC energies, see Tab. 3.2.

Structure of HYDJET++ is illustrated in Fig. 3.1.

Since the programme uses parametrisation of relativistic hydrodynamics rather than a full hydrodynamical calculation, the model is rather efficient and requires relatively little

---

[1]as for March 2015
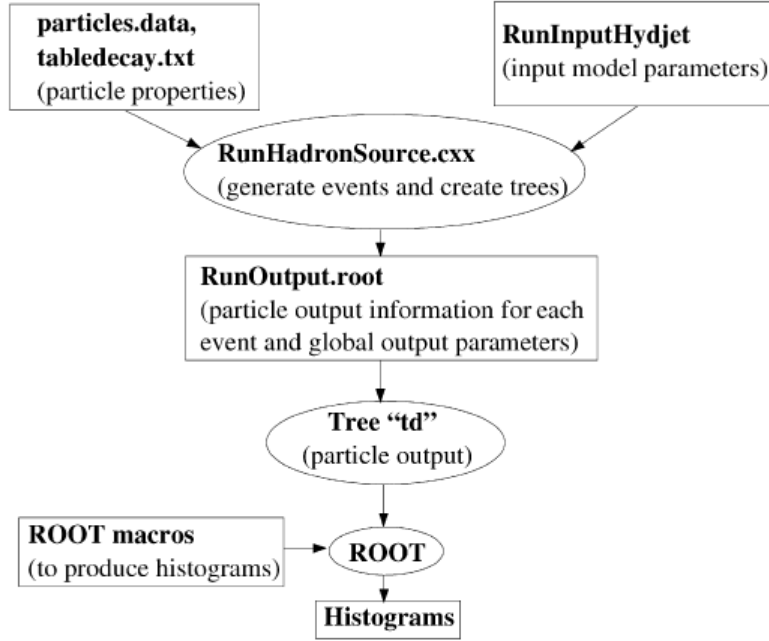
Figure 3.1: Structure of HYDJET++ . Taken from [32]

CPU time to generate enough data. Combining the two independent parts, HYDJET++ is able to reproduce realistic shapes of flow distributions. Last but not least, HYDJET++ contains a vast table of resonances, thus providing a convenient tool for studies of effects of final-state interactions on hadronic flow.

In the soft component of the programme, the elliptic and triangular flow come from modification of the freeze-out hypersurface and of the particle velocities, while in the hard part the v_2 comes from jet quenching. However the later is very small compared to v_2 from the hydrodynamics. The total elliptic flow is naturally a sum of the two components. Elliptic flow is generated through spatial anisotropy $\varepsilon(b)$ and momentum anisotropy $\delta(b)$:

$$
\begin{aligned}
\varepsilon(b) &= \frac{R_y^2 - R_x^2}{R_y^2 + R_x^2} \\
\frac{u^y}{u^x} &= \sqrt{\frac{1 - \delta(b)}{1 + \delta(b)}}\, \tan \phi
\end{aligned}
\tag{3.1}
$$

where R_x and R_y are the projection of the fireball radius onto the x-direction and y-direction respectively and $u^{x,y}$ is the fluid velocity in corresponding direction. The anisotropy parameters $\varepsilon(b)$ and $\delta(b)$ were obtained by fitting the experimental data.

To obtain triangular flow, the radius of the freeze-out surface has to be modified using

an additional triangularity parameter $\varepsilon_3(b)$ as

$$R(b, \phi) = R_f(b) \frac{\sqrt{1 - \varepsilon^2(b)}}{\sqrt{1 - \varepsilon(b) \cos 2\phi}} \left\{ 1 + \varepsilon_3(b) \cos \left[3(\phi - \Psi_3) \right] \right\}. \tag{3.2}$$

The axis Ψ_3 is generated randomly w.r.t. Ψ_2, therefore triangular flow is not correlated with elliptic flow.

3.1.1 Input parameters and files

HYDJET++ is user-controlled by input-file `RunInputHydjet`.

Three pre-set input files are distributed directly with the HYDJET++ package - `RunInputHydjetRHIC200` to be used for simulations as at RHIC Au+Au collisions at $\sqrt{s_{NN}} = 200$ GeV, and `RunInputHydjetLHC2760` and `RunInputHydjetLHC5500` to simulate Pb+Pb collisions at $\sqrt{s_{NN}} = 2.76$ TeV and $\sqrt{s_{NN}} = 5.5$ TeV respectively.

The type of collision is specified by following input parameters:

- number of generated events, `fNevnt`

- energy per nucleon pair $\sqrt{s_{NN}}$ in GeV, `fSqrtS`

- nuclei mass number A, `fAw`

- flag of type of centrality generation, `fIfb`; one can either set a fixed value of the impact parameter b `fBfix` or have b generated between `fBmin` and `fBmax`

- minimum impact parameter in units of nucleus radius R_A, `fBmin`

- maximum impact parameter in units of nucleus radius R_A, `fBmax`

- fixed impact parameter in units of nucleus radius R_A, `fBfix`.

Change of other parameters from their default value is optional.

HYDJET++ permits switching off different types of decays via `fWeakDecay`. This particular input parameter has been modified since the release of HYDJET++ . Instead of simply switching weak decays off, the parameter sets low decay-width threshold (in GeV) - decays with width bellow this value will not be permitted [34]. Typical width for strong, electromagnetic and weak processes are listed in Tab. 3.1. ALICE data have shown unexpected ratios of produced p/π ratios [35], the spectra had to be therefore corrected for weak decays. In the presented work, we set `fWeakDecay` $= 10^{-9}$ for events at LHC energies. In case of the RHIC, `fWeakDecay` $= 0$.

HYDJET++ contains a vast table of resonances, the table can be found in the main folder in file `particle.data`. Decay channels and branching ratios are listed in `tabledecay.txt`.

interaction	typical width [GeV]
weak	10^{-15}
electromagnetic	10^{-6}
strong	10^{-4}

Table 3.1: Typical decay widths for strong, electromagnetic and weak interaction [34].

Each particle can be identified in HYDJET++ by its `pdg1` flag. The flag of particle and its antiparticle are of equal value, but opposite sign. Analogically, the same values used as mother-particle flag `Mpdg1` will provide information of all particles originating in a decay of such particle.

3.1.2   Output

Output of HYDJET++ is written into a ROOT file, recording the entire event history into a TTree `td`. Global parameters describing each event as well as information of all primary particles and their decay products including kinematics of each process are saved into output file specified by user. If no custom file is given, the programme will automatically write into default output file `RunOutput.root`.

It is possible to write the output directly into histograms. In such case one needs to first modifie the macro `RunHadronSourceHISTO.cxx` in order to create histograms one would like to investigate. Unless otherwise specified, running the macro will produce the output file `RunOutputHisto.root`.

3.1.3   Validation of HYDJET++ with experimental data

Validity of HYDJET++ predictions has been achieved through fitting the model to describe various observables in Au+Au data at $\sqrt{s_{NN}} = 200$ GeV from RHIC.

Thermodynamical parameters were obtained from various particle ratios in central collisions near midrapidity (chemical potential μ, chemical freeze-out temperature T_{ch}) and from the slopes of low-p_T hadron spectra (thermal freeze-out temperature T_{th}, maximal transverse flow rapidity at thermal freeze-out y_T^{max}). The proper time τ_0 and maximal transverse radius at thermal freeze-out R_T^{max} were fixed from $\pi^+\pi^-$ correlations.

Particle densities in the midrapidity region and the maximal longitudinal flow rapidity y_L^{max} were derived via fitting the pseudorapidity distributions of charged hadrons from PHOBOS [36]. Comparison of experimental data and HYDJET++ calculations is shown in Fig. 3.2. Relative contributions of the soft and hard components were extracted from the centrality dependence of the η distributions.

Energy loss parameters of the hard component were fixed from high transverse momentum p_T spectra, shown in Fig. 3.3. Reasonable fit of STAR data [37] with HYDJET++

	Pb+Pb $\sqrt{s_{NN}} = 2.76$ TeV	Au+Au $\sqrt{s_{NN}} = 200$ GeV
T_{ch} [MeV]	165	165
μ_B [MeV]	0.0	28.5
T_{th} [MeV]	105	100
τ_0 [fm/c]	12.2	8.0
R_T^{max} [fm]	13.45	10.00
y_L^{max}	4.5	3.3
y_T^{max}	1.265	1.100
p_T^{min}	8.20	3.55

Table 3.2: Values of HYDJET++ input parameters for Pb+Pb collisions at $\sqrt{s_{NN}} = 2.76$ TeV and Au+Au collisions at $\sqrt{s_{NN}} = 200$ GeV: temperature at chemical freeze-out T_{ch}, baryon chemical potential μ_B, temperature at thermal freeze-out T_{th}, maximal transverse radius at thermal freeze-out R_T^{max}, maximal longitudinal flow rapidity at thermal freeze-out y_L^{max}, maximal transverse flow rapidity at thermal freeze-out y_T^{max}, minimal transverse momentum of parton binary collisions p_T^{min}. Taken from current version of HYDJET++.

was achieved assuming $T_0 = 300$ MeV.

The list of current values of parameters for Au+Au at $\sqrt{s_{NN}} = 200$ GeV and for Pb+Pb at $\sqrt{s_{NN}} = 2.76$ TeV can be found in Tab. 3.2.

3.2 Previous HYDJET++ calculations

HYDJET++ has been extensively used to study flow at both RHIC and LHC energies. Here, only a fraction of the already achieved results is discussed.

Figure 3.4 (a) shows p_T dependence of elliptic flow for multiple hadron species measured at STAR and PHENIX in minimum bias Au+Au collisions at $\sqrt{s_{NN}} = 200$ GeV (points) and in HYDJET++ (lines). HYDJET++ simulation agrees well with experimental data in lower $p_T \lesssim 1.5$ GeV/c, excluding the Ξ baryons.

The hydrodynamical part of HYDJET++ does not contain information about the quark phase. Hence it does not have to necessarily observe the scaling. However, the model was fit to describe the measured experimental data (discussed in previous section) in order to yield realistic elliptic flow of identified hadrons. Since the v_2 itself is well described in the simulations, it is then likely to also hold true to the scaling behaviour. Comparison between the measured number-of-constituent-quark scaling and HYDJET++ calculations is shown in Fig. 3.4 (b). The flow of hadrons generated in the model follows approximate NCQ scaling up to $kE_T/n_q \sim 0.7$ GeV. The distribution for Ξ then seems to differ significantly from the rest, this may be explained with multi-strange hadrons being frozen out at earlier stage (see [38] and references therein).
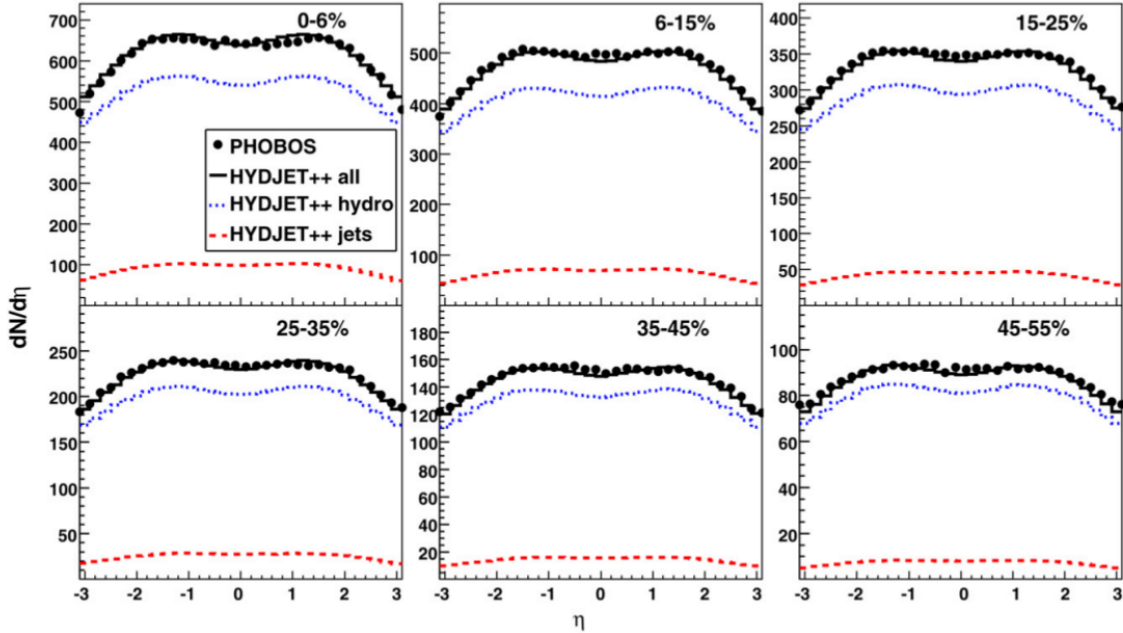
Figure 3.2: dN/dη of charged hadrons in Au+Au collisions at $\sqrt{s_{NN}} = 200$ GeV. HY-DJET++ calculations for hard component, soft part and for the total distribution are denoted by dotted, dashed and solid histograms respectively. Points represent PHOBOS data [36]. Taken from [32].

3.2.1   Triangular flow in HYDJET++

Lately, triangular flow has been added to the model. The parameters were tuned to properly describe LHC data. Comparison between elliptic and triangular flow simulated by HYDJET++ and data from CMS [25] and from ATLAS [26] can be found in Fig. 3.5, top row is v_2 and bottom is v_3. Theoretical calculations can be separated into two groups: "true" values obtained directly from the generator $v_2(\Psi_2^{RP})$ and $v_3(\Psi_3^{RP})$ and from experimental methods such as event plane $v_n\{EP\}$.

HYDJET++ describes both sets of v_2 data well at low transverse momentum $p_T \lesssim$ 1 GeV/c. At higher p_T, however, the model does not correspond to the experiment (although CMS and HYDJET++ agree very well in centrality window $15 - 20\%$, shown in this thesis). In case of the triangular flow, the situation is better.

Given that there is a huge difference in final experimental value of both v_2 and v_3 depending on the method and on the experimental settings, the HYDJET++ model gives a good description of elliptic and triangular flow at LHC energies.
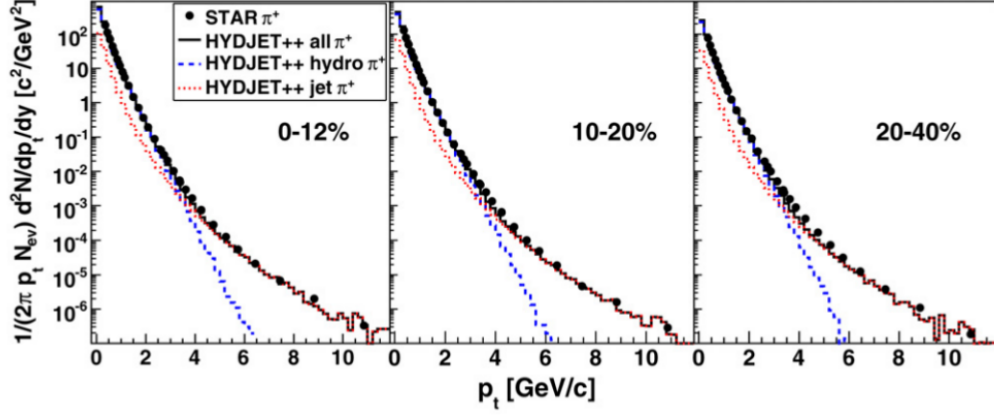
Figure 3.3: p_T-distribution of π^+ in Au+Au collisions at $\sqrt{s_{NN}} = 200$ GeV. HYDJET++ calculations for hard component, soft part and for the total distribution are denoted by dotted, dashed and solid histograms respectively. Points represent STAR data [37]. Taken from [32].

(a)   (b)
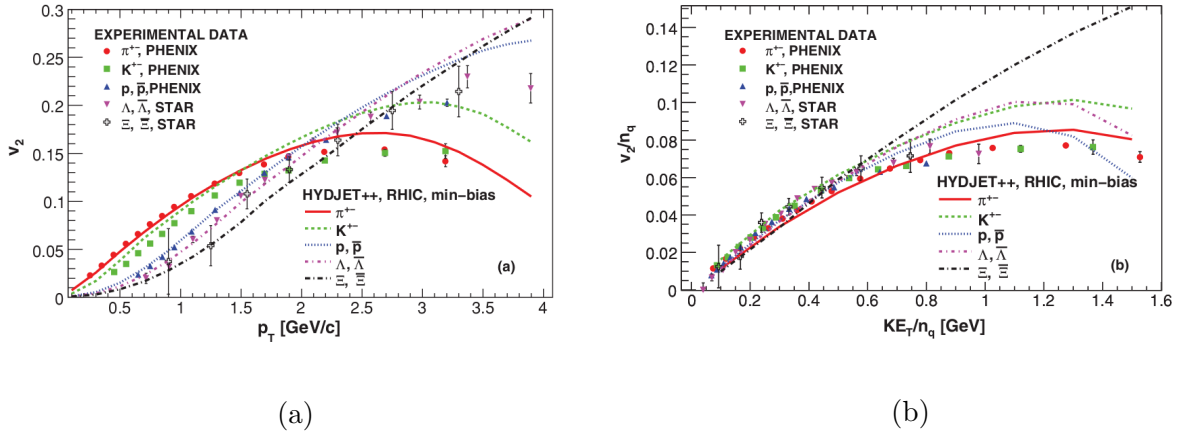
Figure 3.4: (a) $v_2(p_T)$ for different hadron species in HYDJET++, compared with RHIC data from Au+Au collisions at $\sqrt{s_{NN}} = 200$ GeV. (b) v_2/n_q vs kE_T/n_q for the same settings. Taken from [38].
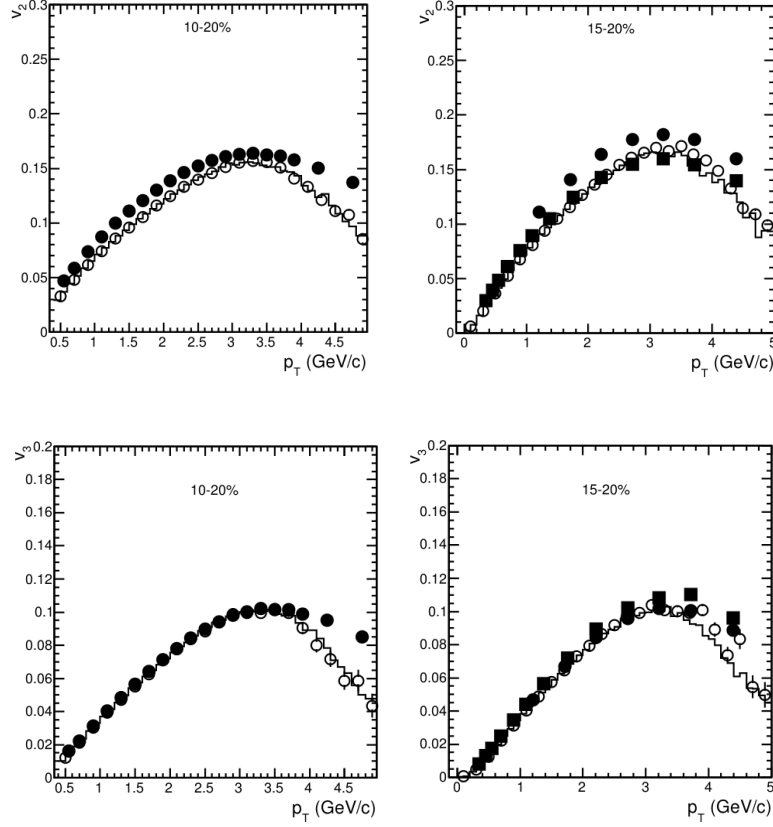
Figure 3.5: Elliptic flow $v_2(p_T)$ (top) and triangular flow $v_3(p_T)$ (bottom) of charged hadrons in Pb+Pb collisions at $\sqrt{s_{NN}} = 2.76$ TeV, comparing HYDJET++ calculations with ATLAS at $10-20\%$ (left) and CMS at $15-20\%$ (right) data [26, 25]. The histogram and open circles represent v_2 and v_3 from HYDJET++ obtained by two different methods. Full circles denote the experimental data. Taken from [40].

Chapter 4

Simulations of flow at LHC

We performed a study of triangular flow at LHC and RHIC energies. About 1M events were generated in total for each data set. As HYDJET++ contains a vast table of resonances and information about their decays, influence of final-state effects on triangular flow has also been investigated. Calculations for Pb+Pb collisions at $\sqrt{s_{NN}} = 2.76$ TeV were compared to ALICE [23] and CMS data [25](for both, $|\eta| < 0.8$). Ratio of triangular flow to elliptic flow at LHC was compared with ATLAS data in pseudorapidity window $|\eta| < 2.5$ [26].

In the experiment, distributions for charged particles are usually substituted by distributions for the most abundant charged particles, i. e. protons, pions and kaons. As their numbers should by far exceed number of other particles created in studied processes, the two distributions should be essentially the same. The same assumption was employed in present calculations, meaning that by *all charged* particles, we imply all protons, pions and kaons and their antiparticles. Analogically, Λ-distributions are calculated as distributions for two states, i. e. $\Lambda^0(1115)$, $\Sigma^0(1192)$ and their respective antiparticles. This is due to the fact that all Σ^0 decay electromagnetically into Λ^0 [41]. Those then contribute to the total flow of Λ baryons and need to be taken into account.

Tab. 4.1 sums up the states which were taken into account for charged particles and for Λs.

4.1 Statement of aurhor's contribution

Author of the presented thesis performed the full calculations in HYDJET++ shown in the current and the following chapters. They modified the appropriate macros in order to receive flow distributions discussed in following text, for both Pb+Pb at $\sqrt{s_{NN}} = 2.76$ TeV and Au+Au at $\sqrt{s_{NN}} = 200$ GeV. The aim of the study was to investigate the triangular flow and how it is influence by decays of resonances, done separately for RHIC and for LHC energies. The author then compared the simulations with available experimental data to interpret the results. Such study has never been performed before.

	particles	mass $[\text{GeV}/c^2]$	quark content	Abs(pdg1)
charged	$(p + \bar{p})$	938.272046 ± 0.000021	(uud)	2212
	$\pi^\pm$	139.57018 ± 0.00035	$(u\bar{d})$	211
	$K^\pm$	493.677 ± 0.016	$(u\bar{s})$	321
$\Lambda, \bar{\Lambda}$	$\Lambda^0 + \overline{\Lambda^0}$	1115.683 ± 0.006	(sud)	3122
	$\Sigma^0 + \overline{\Sigma^0}$	1192.642 ± 0.024	(sud)	3212

Table 4.1: Particle states used for charged and lambda distributions. The states are uniquely identified in HYDJET++ via `pdg1` flag. Displayed content for either baryon or positive meson only.

4.2   Triangular flow at the LHC

Figure 4.1 shows triangular flow as a function of transverse momentum in Pb+Pb collisions at $\sqrt{s_{NN}} = 2.76$ TeV in centrality window $10 - 30\%$, divided into four bins, compared with data from the CMS experiment [25]. The calculations are in a rather good agreement at low transverse momentum up to $p_T \sim 2.5 - 3.0$ GeV/c. The model is less successful at higher p_T, yet it is still able to provide realistic shape of the distribution - the flow does not infinitely grow with p_T but rather decreases after reaching a maximum. The shape of the distribution does not change significantly with centrality.

Let us now explain what are the individual distribution in some of the next figures, denoted by "direct", "hydro" and "jets" (and combinations):

direct means that only particles that are produced directly through hadronisation or from jet fragmentation are considered. In other words, they have no mother particle and come from no decay. In experiment, the term "primary" may be used to describe such particles, for consistence with previous work on flow within HYDJET++ , we will keep to the term direct.

hydro signifies that only hadrons generated in the soft - hydro - component are considered. They include hadrons coming from decays of resonances, unless otherwise indicated.

jets denotes hadrons from the hard component, created from jets. They may include hadrons originating from decays of heavier particles, unless otherwise indicated.

hydro+jets is a different name for the total distribution, where both components are used to generate particles. Occasionally the term "all hadrons" will be used to describe such distribution.

Comparison between the soft part and the hard part and the total distribution can be found in Fig. 4.2. Full circles show triangular flow distribution for all charged particles calculated
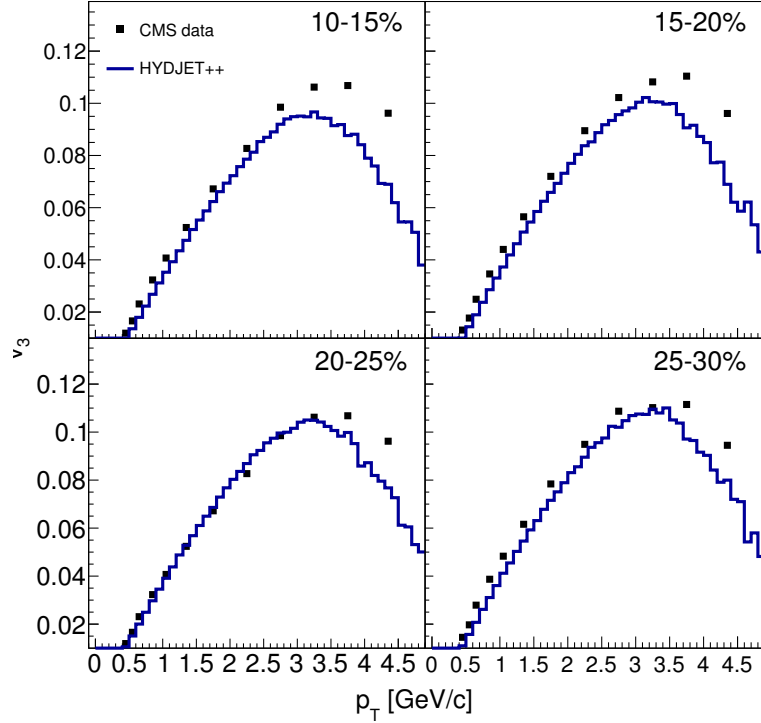
Figure 4.1: Triangular flow in Pb+Pb at $\sqrt{s_{NN}} = 2.76$ TeV (black squares) measured by the CMS experiment [25] and in HYDJET++ (blue line) for centrality $10 - 30\%$. Method used to treat presented data is described in [25] and references therein.

with HYDJET++. Histograms represent flow coming from the hydrodynamics (blue solid line), from jets (black dashed line) and from combined calculation for direct particles only (red dashed line). The observed rise in flow is due to hydrodynamics, however already at low p_T, the real distribution starts to deviate from the hydro-calculation. At high p_T the majority of particles are produced from jets, which carry little flow, thus explaining the fall in the distribution. The distribution for direct charged particles follows a pattern similar to all charged particles.

Distributions of triangular flow generated for single species are displayed in Fig. 4.3. The upper plot (a) shows the total triangular flow as a function of p_T, i. e. combining hadrons from the soft and from the hard part of the programme. The hadrons form the so-called meson and baryon branches. At low p_T, we see that the mass ordering, explained in Sec. 1.3.1, takes place. With growing p_T, one observes crossing of the two branches followed by fall-off. Flow of hadrons generated only in the soft part, driven by parametrisation of hydrodynamics, is pictured in the bottom plot (b). In conclusion, the mass ordering can be explained with hydrodynamical approach. To obtain the subsequent crossing of meson and baryon branches, jets need to be included.
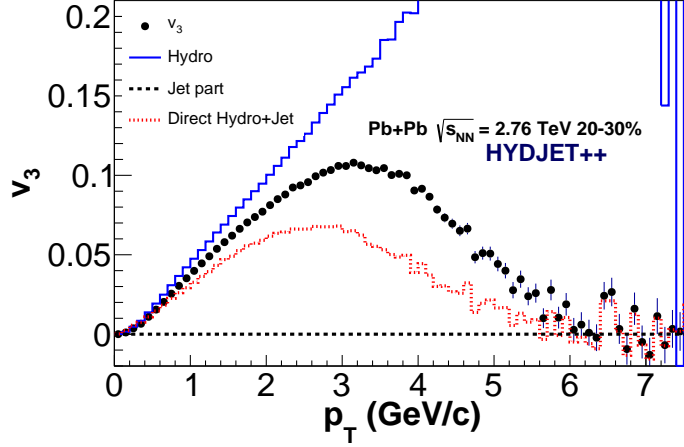
Figure 4.2: The total triangular flow distribution $v_3(p_T)$ in Pb+Pb at $\sqrt{s_{NN}} = 2.76$ TeV (full circles). Histograms show distributions of hydrodynamical flow (blue solid line), flow of hadrons produced in jets (black dashed line) and flow of direct hadrons (red dotted line).

As mentioned in Sec. 2.1, the ratio of $v_3^{1/3}(p_T)/v_2^{1/2}(p_T)$ should bear very little p_T dependence. The magnitude of the distributions should however change with centrality. Figure 4.4 shows the ratio $v_3^{1/3}/v_2^{1/2}$ vs p_T in Pb+Pb collisions at $\sqrt{s_{NN}} = 2.76$ TeV in HYDJET++ for four centrality intervals between $0 - 30\%$, compared to ATLAS data [26] as in Fig. 2.5a. The uncertainties for ATLAS data were calculated as

$$\sigma = \sqrt{\sigma_{stat}^2 + \sigma_{sys}^2},$$

where σ_{stat} and σ_{stat} denote statistical and systematic uncertainty respectively.

The ratio does indeed display centrality dependence. The distributions obtained from HYDJET++ are rather flat in p_T. The ATLAS data, on the other hand, indicate a weak variation with transverse momentum, the ratio is marginally growing with p_T.

$v_3^{1/3}/v_2^{1/2}$ computed with HYDJET++ exceeds the central value for the ratio obtained from the data in all studied centrality windows. For the most central events, $0 - 5\%$ and $5 - 10\%$, the two distributions agree within uncertainties. For the centrality windows $10 - 20\%$ and $20 - 30\%$ in transverse momentum range $p_T = 0 - 2.5$ GeV/c, HYDJET++ predicts significantly greater value for the ratio than suggested by ATLAS, yet agree for $p_T > 2.5$ GeV/c.

To trace the origin of this discrepancy, we have plotted the elliptic and triangular flow p_T-distribution for the $10 - 20\%$ centrality window, see Fig. 4.5. Similar plots can be found in [40]. While the computed v_3 is in rather good agreement to the experimental points, the distributions of v_2 do differ greatly. As discussed in Sec. 3.2, this comes from
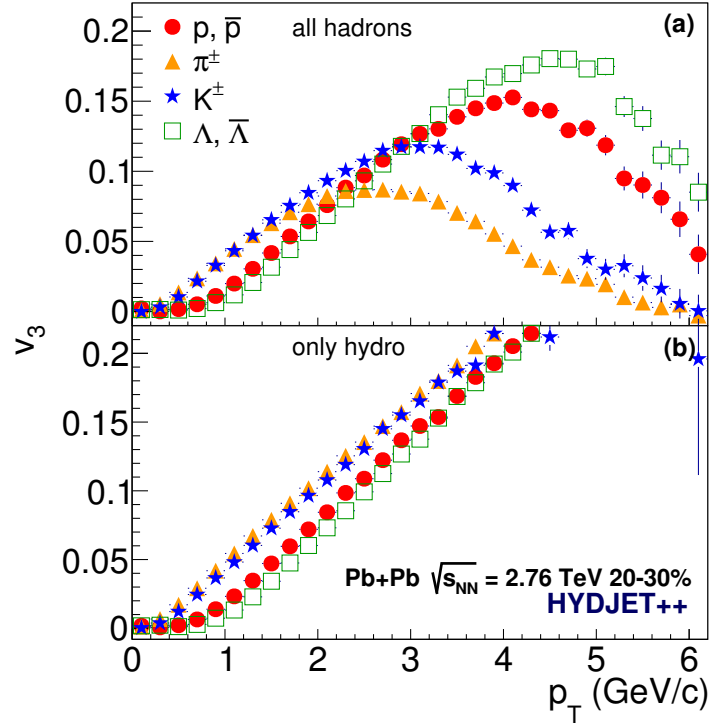
Figure 4.3: (a) $v_3(p_T)$ distributions for protons (full red circles), pions (yellow triangles), kaons (blue stars) and Λ baryons (open green squares) in Pb+Pb at $\sqrt{s_{NN}} = 2.76$ TeV in HYDJET++. (b) $v_3(p_T)$ distributions for hydro-part only.

the method used during treatment of data. Bearing this in mind, it is safe to state that the ratio computed with HYDJET++ is in reasonable agreement with experimental value.

4.3 Effect of final-state interactions on v_3

Study of effects of resonance decays on triangular flow was performed. Results of our calculations can be found in Fig. 4.6. For each species, v_3 distributions for all particles are compared to distributions for direct particles only. Decays of resonances change the shape significantly: the maximum of the distribution is shifted to higher p_T, its amplitude is raised. The effect is stronger for lighter particles. Subfigures (b) (d) show the distributions for Λ baryon and π meson respectively. For the latter, the amplitude is raised nearly by factor 2, the shift in p_T is approximately ~ 1 GeV/c. In the case of Λ, the p_T-shift is still rather significant (~ 1 GeV/c as in previous case), however the amplitude in the maximum of the distribution does not change so drastically.

To study decay kinematics in order to explain the observed shift if resonances are counted in, we have drawn $v_3(p_T)$ distribution of direct pions and protons and of those
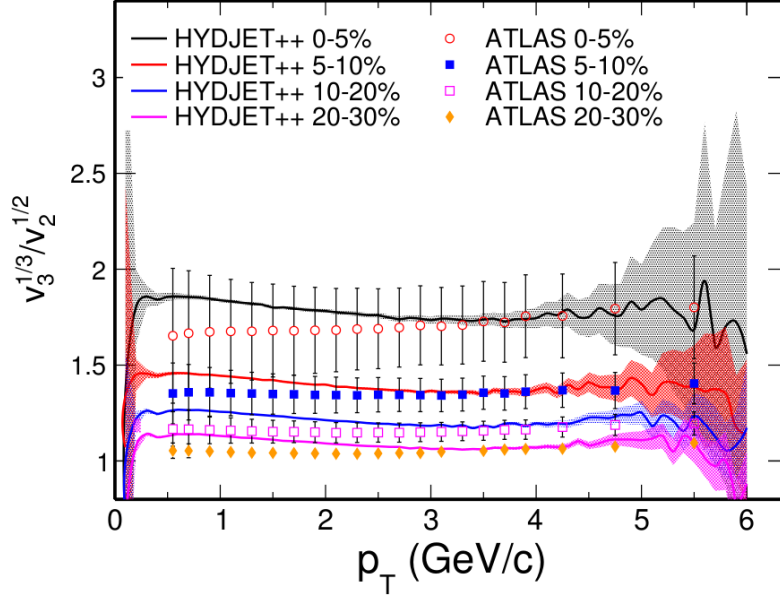
Figure 4.4: The ratio $v_3^{1/3}/v_2^{1/2}$ as a function of p_T for several centrality intervals in the range of $0 - 30\%$. HYDJET $++$ calculations (lines) are compared with data from the ATLAS experiment [26]. Bands denotes statistical uncertainty.

coming from decays of given resonances (the resonances and used decay channels are listed in Tab. 4.2) and compared them with triangular flow of the original resonance species, see Fig. 4.7. Flow of π coming from decays of ρ mesons are shown in panel (a) together with the distribution of the original meson resonance. We see that the two distributions look more or less similar, both considering the amplitudes and the transverse momenta in their respective maxima,

$$v_3^\rho(p_T) \sim v_3^\pi(p_T), \tag{4.1}$$

while in the case of a three-body decay such as $\omega \longrightarrow \pi\pi\pi$, the resulting decay-pion distribution is remarkably softer:

$$v_{3,max}^\omega \approx v_{3,max}^\pi \tag{4.2}$$

$$\langle p_T^\omega \rangle > \langle p_T^\pi \rangle. \tag{4.3}$$

The picture is quite different in case of baryon resonances. Panels (c) and (d) compare the flow of Δ with flow of pions and protons (both coming from its decays and direct) respectively. Generally, when a heavy resonance decays into a proton and a pion, most of its p_T is carried by the proton. The pion, on the other hand, is produced at low p_T and hence

$$\langle p_T^{\text{resonance}} \rangle \approx \langle p_T^p \rangle > \langle p_T^\pi \rangle. \tag{4.4}$$
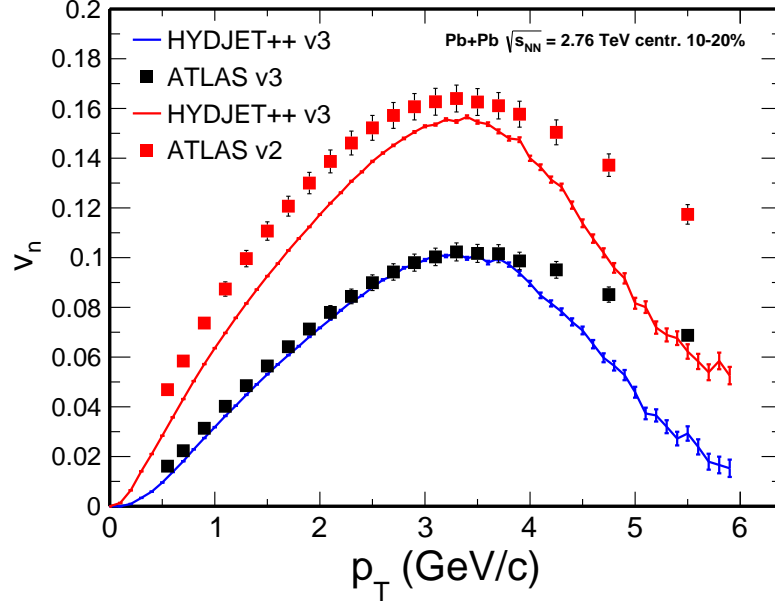
Figure 4.5: p_T distributions of elliptic and triangular flow in Pb+Pb at $\sqrt{s_{NN}} = 2.76$ TeV at centrality $10-20\%$. Lines show distribution obtained with HYDJET++ , points denote ATLAS data [26].

The magnitude of triangular flow $v_{3,max}$ is about the same for the resonance and for its decay products:

$$v_{3,max}^{\text{resonance}} \approx v_{3,max}^{p} > v_{3,max}^{\pi}. \tag{4.5}$$

Focusing on the p_T shift, we see that in case of ρ meson (Fig. 4.7(a)), as well as in case of Δ baryon (c), we observe

$$\langle p_T^{\pi\ direct} \rangle_{\rho,\ \Delta} \approx \langle p_T^{\pi\ decay} \rangle_{\rho,\ \Delta}. \tag{4.6}$$

On the other hand, there is a visible shift in case of ω and thus

$$\langle p_T^{\pi\ direct} \rangle_{\omega} < \langle p_T^{\pi\ decay} \rangle_{\omega}. \tag{4.7}$$

Naturally, when all possible decays are summed up, the maximum of the corresponding distribution will be shifted to higher p_T. Unlike on case of v_2 [38], the direct distribution does not exceed the distribution with decays - this appears to be balanced by such decays as $\rho \longrightarrow \pi\pi$ and $\Delta \longrightarrow p\pi$ hereby discussed.

We also studied the NCQ scaling of v_3 at LHC, taking into consideration both scenarios: scaling as v_3/n_q, investigated by ALICE [24] and as $v_3/n_q^{3/2}$ studied at STAR [21].

The scaling picture as in the first scenario, v_3/n_q, is shown in Fig. 4.8. The top left-most plot (a) shows the direct hydro+jets v_3/n_q vs kE_T/n_q for proton, kaons, pions and Λs. There is no NCQ scaling. However, once the particles originating in decays are

hadron	quark content	mass [MeV/c^2]	decay channels	Γ_j/Γ [%]	|pdg1|
ω	$(1/2(u\bar{u} + d\bar{d}))$	782.65 ± 0.12	$\pi^+ + \pi^- + \pi^0$	89.2 ± 0.7	223
			$\pi^+ + \pi^-$	1.53 ± 0.13	
ρ^0	$(1/2(u\bar{u} - d\bar{d}))$	775.49 ± 0.34	$\pi^+ + \pi^-$	~ 100	113
ρ^+	$(u\bar{d})$	775.49 ± 0.34	$\pi^+ + \pi^0$	~ 100	213
Δ^{++}	(uuu)	1232 ± 2	$p + \pi^+$	$*$	2224
Δ^+	(uud)	1232 ± 2	$p + \pi^0$	$*$	2214
			$\eta^0 + \pi^+$	$*$	
Δ^0	(udd)	1232 ± 2	$p + \pi^-$	$*$	2114
Δ^-	(ddd)	1232 ± 2	$\eta^0 + \pi^-$	$*$	1114

Table 4.2: Examples of resonances and their characteristics. Listed are decay channels relevant for present study. Mass and branching ratio Γ_j/Γ were taken from [41]. In case of Δ baryons, $\Gamma(\Delta \longrightarrow N\pi)/\Gamma_{total} = 100\%$

counted in, the situation improves, as can be seen in (b). Here the total distributions are displayed. Distributions for individual particles lie closer one to another. To study the role of the two independent parts, hydro and jets, we have plotted the distribution for hadrons generated in the soft hydro component only. Distributions show clear scaling behaviour, although pions are a bit bellow the other species. The point is more obvious from plots (d), (e) and (f), which show the same distributions as (a), (b) and (c) respectively, only this time divided by the corresponding proton distribution. The bottom plots are however only plotted for reader's comfort, errors are not shown.

The calculations suggest that the NCQ scaling comes from the final state interactions of the hadrons created in the medium rather than from the partonic phase. Decays of resonances created from the thermalised medium drive the flow towards scaling. Jets, on the other hand, seem to add to the breaking of the scaling at LHC energies.

Fig. 4.9 show a similar picture for $v_3/n_q^{3/2}$ vs kE_T/n_q distributions, the plot order and legend follow the same system as the previous plot. As in the case of $v_3/n_q(kE_T/n_q)$, the distributions for direct particles do not scale at all (plots (a), (d)). Adding hadrons coming from the decays of resonances (see plot (b), (e)), one can see hints of scaling. The scaling picture for $v_3/n_q^{3/2}$ is however significantly worse than for v_3/n_q. Counting in hadrons originating in jets, the scaling is visibly worsened (see (c), (f)).

It is worth to discuss whether our results truly prove the observed scaling to be a sign of flow development at partonic level. HYDJET++ does not contain any information about the partonic phase. Yet the results show hints of scaling, similar to experimental data. Admittedly, one might say that the scaling comes "for free", because no scaling assumptions were implemented in the model "by hand".

4.4   Conclusions

We have shown that

- HYDJET++ gives good predictions of experimental data at LHC energies,

- realistic shape of distributions is achieved through the interplay of hydrodynamics and jets,

- mass-ordering and initial rise of the distributions can be explained by hydrodynamics while the subsequent fall-off and branch crossing is caused by jets,

- ratio $v_3^{1/3}/v_2^{1/2}$ shows strong centrality dependence and is rather flat in p_T;

- the final-state interactions:

  - influence measured flow distributions rather significantly - they increase the magnitude and shift the maximum of the distribution into higher p_T,

  - these effects are more pronounced for lighter particles than for heavier;

- for both NCQ scaling scenarios, $v_3/n_q^{3/2}$ and v_3/n_q,

  - HYDJET++ predicts hints of scaling behaviour,

  - decays of resonances drive flow towards scaling fulfilment, jets distort it.
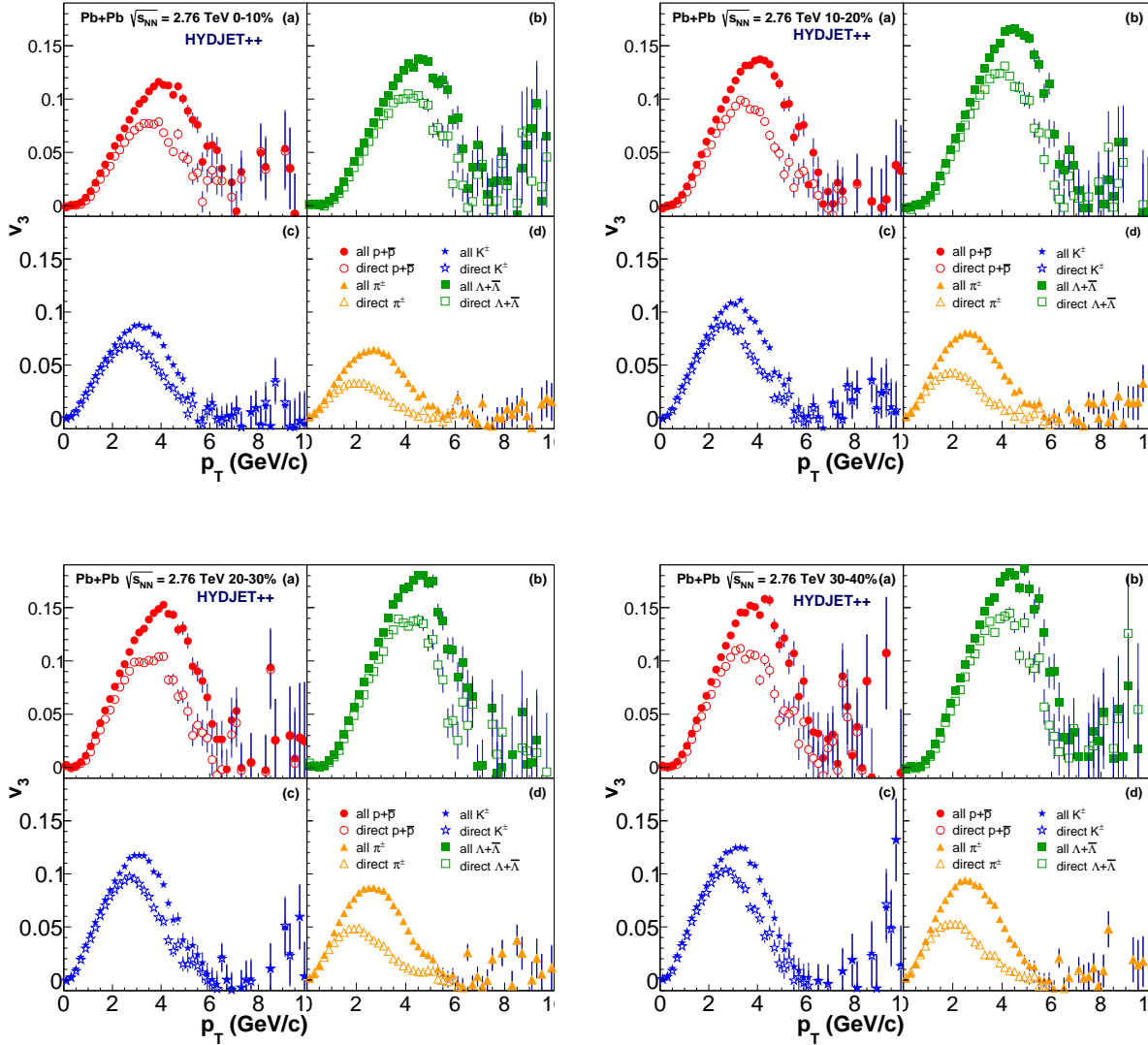
Figure 4.6: $v_3(p_T)$ distributions for all particles (full symbols) and for direct particles (open symbols) in HYDJET++ in Pb+Pb at $\sqrt{s_{NN}} = 2.76$ TeV for different centrality bins: (top left) 0 - 10%, (top right) 10 - 20%, (bottom left) 20 - 30%, (bottom right) 30 - 40%.
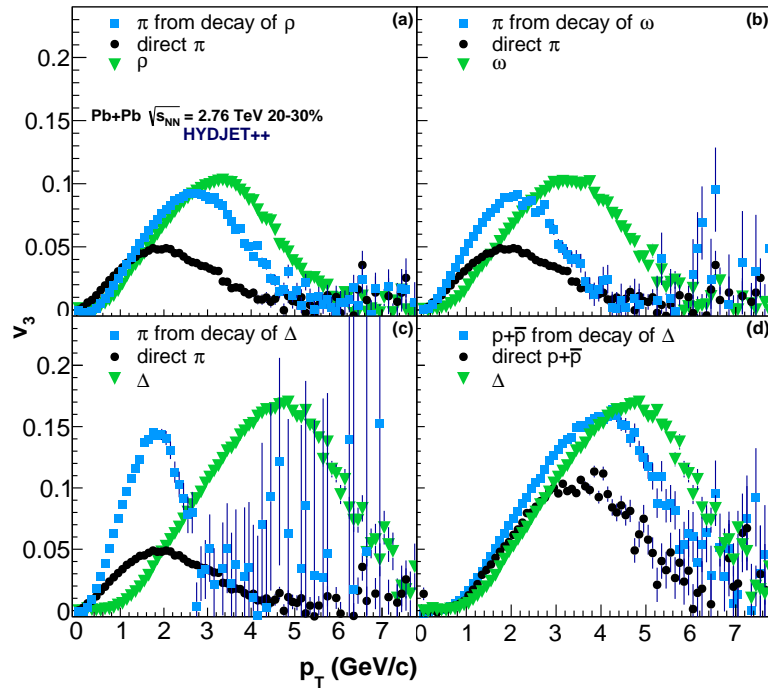
Figure 4.7: (a) $v_3(p_T)$ distribution of charged pions originating in decay of ρ^0 and $\rho^\pm$ (blue squares), direct $\pi^\pm$ (black circles) and of ρ mesons (green triangles). (b) and (c) show similar plots for ω and Δ baryons respectively. (d) shows $v_3(p_T)$ distribution of protons, either direct or coming from decays of Δ.
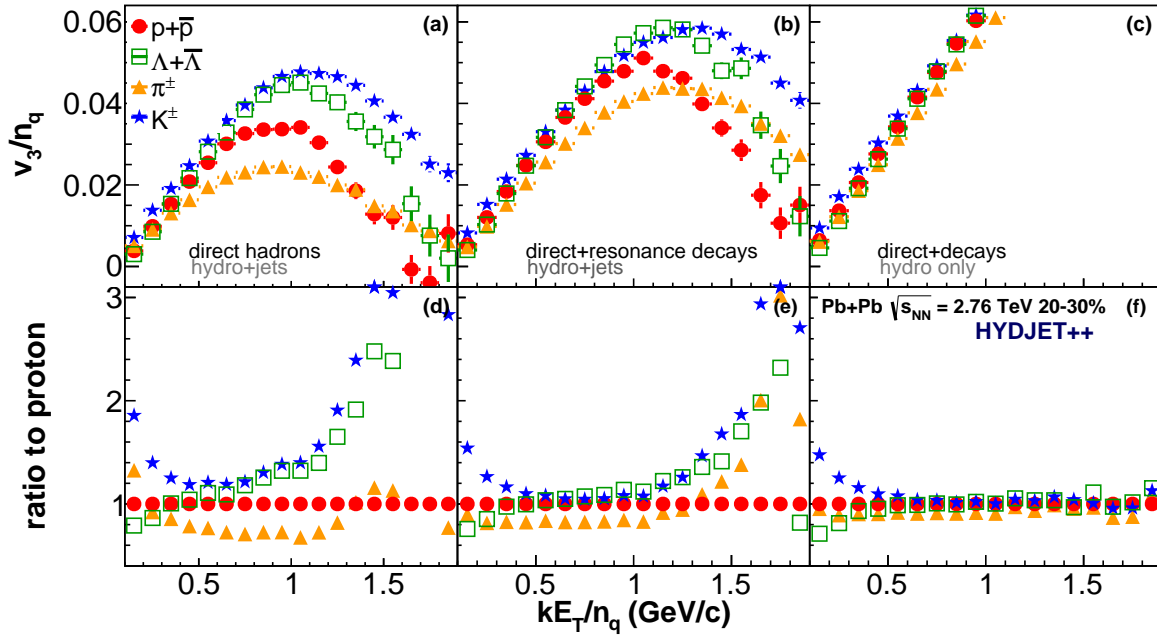
Figure 4.8: (a) v_3/n_q as a function of kE_T/n_q for direct particles only in Pb+Pb collisions at $\sqrt{s_{NN}} = 2.76$ TeV at centrality 20-30% in HYDJET++. (b) v_3/n_q vs kE_T/n_q for all hadrons from hydro+jets. (c) $v_3/n_q(kE_T/n_q)$ for direct particles together with particles coming form decays of resonances, soft component (hydro) used exclusively. (d), (e) and (f) show the distributions drawn on (a), (b) and (c) respectively divided by the corresponding proton distribution.
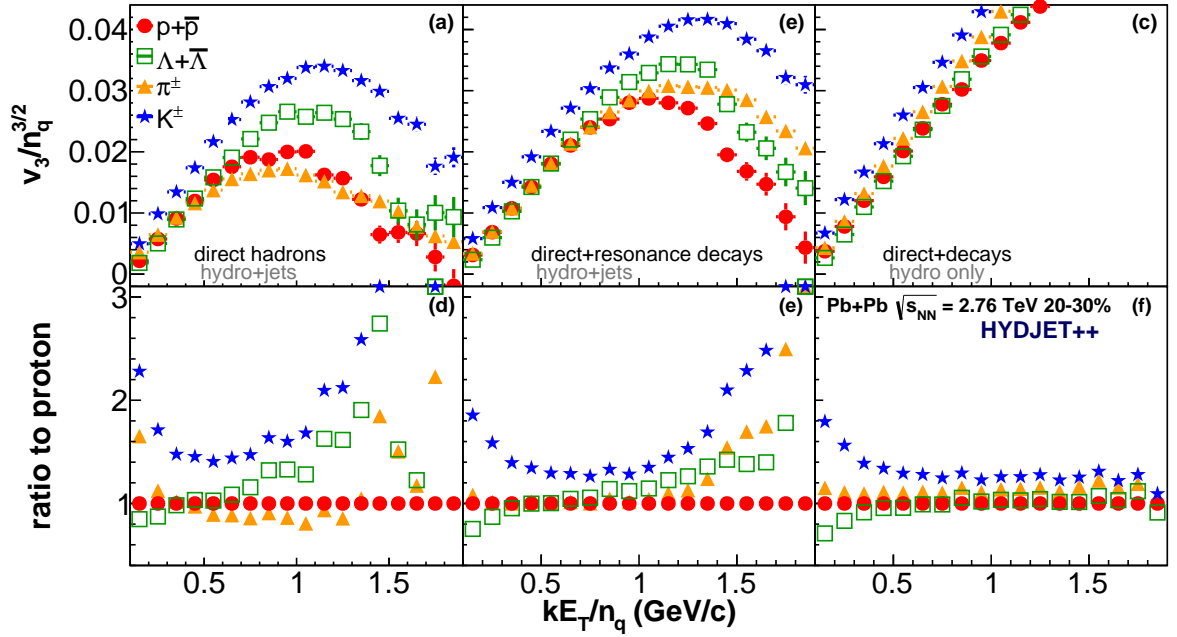
Figure 4.9: $v_3/n_q^{3/2}$ vs kE_T/n_q (a) $v_3/n_q^{3/2}$ vs kE_T/n_q for direct particles only in Pb+Pb collisions at $\sqrt{s_{NN}} = 2.76$ TeV at centrality 20-30% in HYDJET++. (b) $v_3/n_q^{3/2}$ vs kE_T/n_q for all hadrons from hydro+jets. (c) $v_3/n_q^{3/2}$ vs kE_T/n_q for direct particles together with particles coming form decays of resonances, soft component (hydro) used exclusively. (d), (e) and (f) show the distributions drawn on (a), (b) and (c) respectively divided by the corresponding proton distribution.

Chapter 5

Simulations of flow at RHIC

5.1 Triangular flow at RHIC

Triangular flow for different species in Au+Au collisions at $\sqrt{s_{NN}} = 200$ GeV calculated with HYDJET++ over the whole centrality range is shown in Fig. 5.1a . The red circles denote protons, yellow triangles pions and blue stars represent kaons. The proton and pion distributions seem[1] to correspond to recent STAR measurement [28], see Fig. 5.1b. The kaon distribution in HYDJET++ however differs greatly from the STAR data. The calculation yields significantly stronger triangular flow of kaons, the branching is more pronounced. The data show stronger mass ordering than HYDJET++ calculations. The crossing of the two branches occurs at $p_T \sim 2.0$ GeV/c, which is in agreement with the STAR data.

Observed distributions are also affected by decays of resonances, as previously discussed in the case of the LHC. Comparison between total v_3 distribution and the distribution for direct hadrons only is shown in Fig. 5.2. Distributions for unidentified hadrons are displayed in panel (a). Decays of resonances do remarkably increase the magnitude of the flow and they provoke a shift of the maximum of the distribution into harder p_T. This is again caused by the decay kinematics - when the original heavy resonance produces hadrons with higher p_T than those coming directly from the medium. Panels (b), (c) and (d) show the same but for identified hadrons: protons, kaons and pions respectively.

Figure 5.3 shows the $v_3/n_q^{3/2}$ vs p_T for STAR data. The plots for distributions of direct hadrons, direct hadrons together with resonance-decays products from hydro+jets and all hadrons from hydro part only are shown in plots (a, d), (b, e) and (c, f) respectively, following the same system as in Fig. 4.8 and 4.9. Similar as in case of LHC, decays of resonances drive the flow distributions towards fulfilment of NCQ scaling. However, jets at RHIC are less energetic compared to LHC. Therefore they do not distort the the flow as much and thus flow scales even if jets are included.

---

[1]Hereby used wording is deliberate and very important. The data are not yet published and thus direct comparison has not been performed.

(a)

(b)
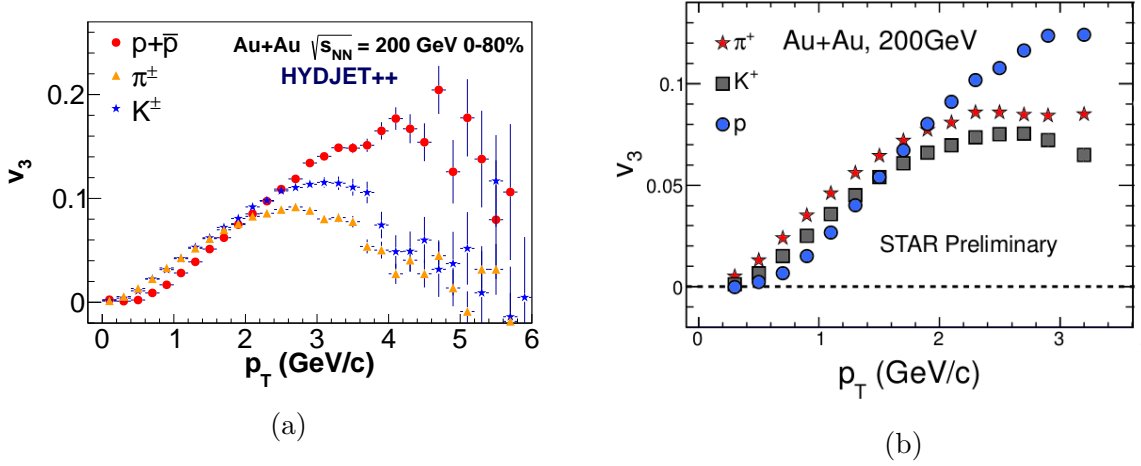
Figure 5.1: (a) Triangular flow $v_3(p_T)$ of identified hadrons in Au+Au collisions at $\sqrt{s_{NN}} = 200$ GeV in HYDJET++ . Red circles denote protons, blue stars kaons and yellow triangles show pions. (b) $v_3(p_T)$ of identified particles measured at the STAR experiment in Au+Au collisions at $\sqrt{s_{NN}} = 200$ GeV Taken from [28].

5.2 Elliptic flow at RHIC

Current version of HYDJET++ was developed to describe the LHC data. Comparison with experimental results was not performed. It might be that the newest version does not describe the flow at RHIC energies correctly, thus explaining the discrepancy between the flow distribution of charged kaons in HYDJET++ and in STAR data. Alternatively, different constraints, not explicitly listed in the conference proceedings [28], may have been applied in STAR analysis than in HYDJET++ simulations.

To investigate the discrepancy between the flow of kaons reported by the STAR and obtained from HYDJET++, a brief inspection of elliptic flow in 200 GeV Au+Au collisions was done. The distributions are plotted in Fig. 5.4a. Comparison with published data from PHENIX is also shown, see Fig. 5.4b. Here we see that the flow obtained in HYDJET++ is much stronger than what was measured by PHENIX. Experimental and theoretical distributions for protons (red circles and red line) and pions (yellow triangles and black line) agree up to $p_T = 1$ GeV/c, but deviate greatly at higher p_T. Distributions for kaons do not agree at all, similar as in the case of v_3 discussed in Sec. 5.1.

Arguably, this issue needs to be studied further in more detail to determine why such inconsistency is observed. One reason may be that not all conditions and cuts applied during the analysis of the data collected by the two experiments at the RHIC were taken into consideration. Or the updated model is less fit for running calculations at RHIC energies. The modification done to describe flow harmonics at the LHC have not been validated with calculations at RHIC energies. The most straightforward way would be to
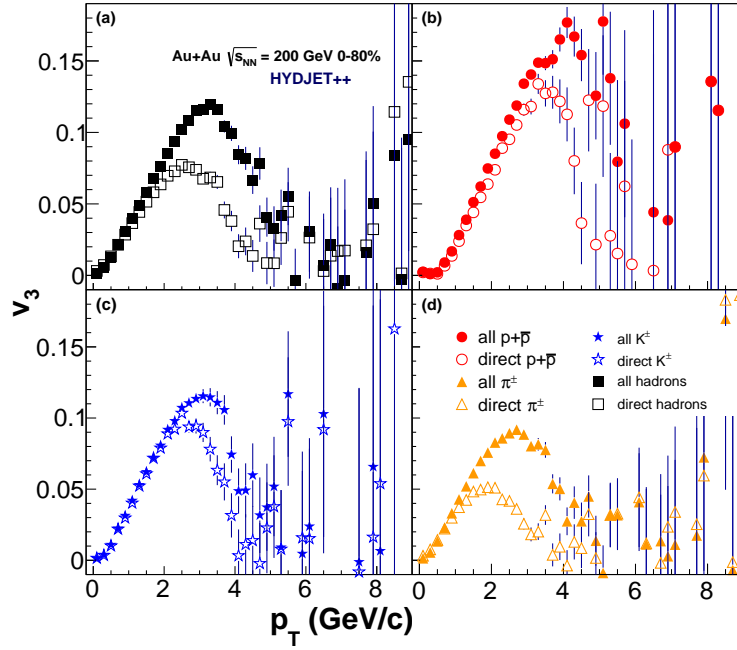
Figure 5.2: $v_3(p_T)$ distributions for all particles (full symbols) and for direct particles (open symbols) in HYDJET++ in Au+Au collisions at $\sqrt{s_{NN}} = 200$ GeV for (a) unidenitfied hadrons, (b) protons, (c) kaons, (d) pions.

compare for instance p_T spectra as was done with previous version, as can be seen in Fig. 3.3.

5.3   Conclusions

Based on our calculation, we came to the following conclusions on triangular flow:

- experimental distributions of v_2 and v_3 at RHIC energies do not agree as well with HYDJET++ as calculations at LHC energies;

- calculated $v_3(p_T)$ of protons and charged pions appears to match the preliminary STAR data at first glance, new study needs to be performed once data is available;

- HYDJET++ yields much stronger $v_3(p_T)$ of charged kaons than is observed in experiment;

Decays of resonances influence measured flow in an important way. Namely,

- as was observed in previous chapter, $v_3(p_T)$ distributions experience both increase in the magnitude of its maximum and its shift to higher p_T due to the decays;
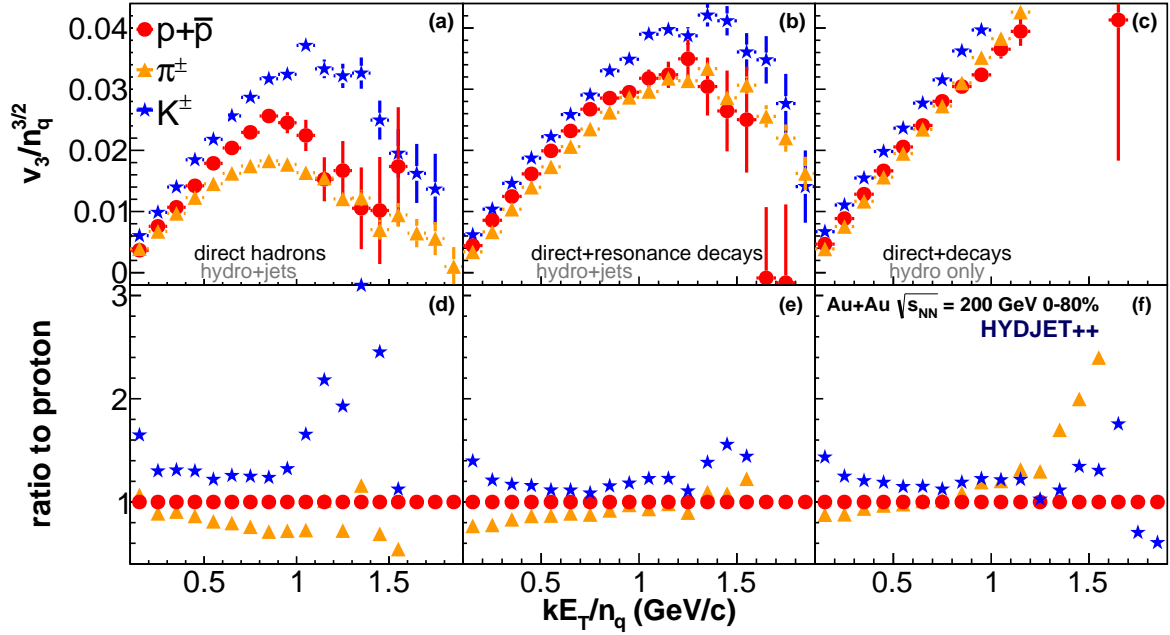
Figure 5.3: $v_3/n_q^{3/2}$ vs kE_T/n_q distributions for protons (red circles), pions (yellow triangles) and kaons (blue stars) in Au+Au collisions at $\sqrt{s_{NN}} = 200$ GeV in HYDJET++ .

- resonances influence the scaling - once they are taken into account, scaling seems to hold true;

- the jets are much less energetic and much less abundant than at the LHC, hence they do not act enough upon the flow to distort the scaling.

Elliptic flow in HYDJET++ differs outstandingly from v_2 measured by the PHENIX experiment, although the respective distributions for pions and protons appear to be consistent in both theory and experiment. Further detailed study is necessary to understand better this issue.

(a)   (b)
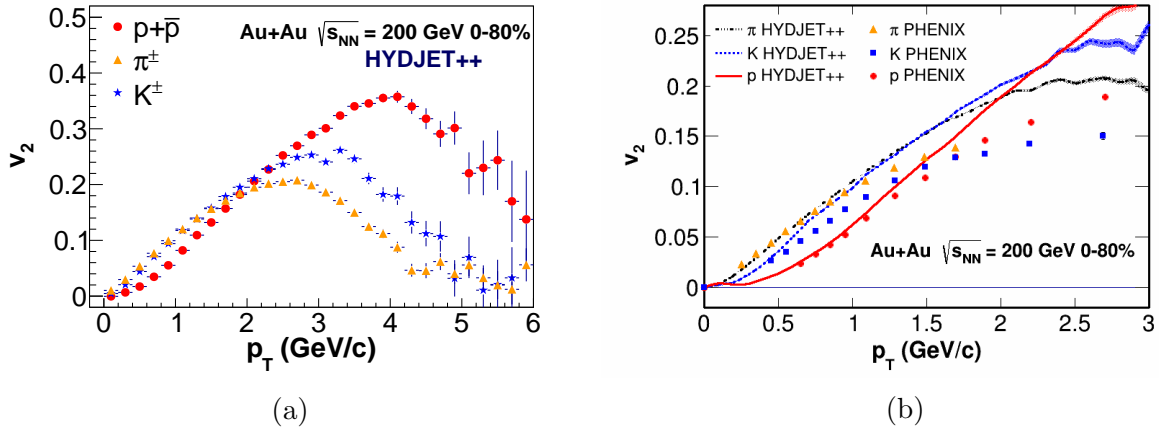
Figure 5.4: (a) Elliptic flow $v_2(p_T)$ in Au+Au collisions at $\sqrt{s_{NN}} = 200$ GeV in HY-DJET++ . Red circles denote protons, blue stars kaons and yellow triangles represent pions. (b) Comparison between HYDJET++ simulations (lines) and PHENIX data [22] (points).

Summary

Relativistic collisions of heavy nuclei recreate the hot and dense matter, present immediately after the Big Bang - the quark-gluon plasma. The state of deconfined quarks and gluons is very short-lived and thus cannot be directly studied. Instead, number of possible signatures of its presence in the system was suggested.

Flow is a prominent sign of collective behaviour of the medium created in such collisions, suggesting thermalised state of matter. In such system, pressure is developed and its gradient cause outward motion of matter, which can be better studied through Fourier expansion of azimuthal distribution of detected particles. Elliptic flow, represented by the second Fourier coefficients v_2, arises from the initial asymmetry of the reaction zone (as all other even v_n do) and was found to be the most important contribution to anisotropic flow at RHIC energies. Since at the LHC, energy density and multiplicity is much higher, higher flow coefficients $n \geq 3$ grow significantly in importance and can be this studied. It was found that the triangular flow, given by the third Fourier coefficient v_3, is the dominant flow harmonic in the most central collisions of $Pb + Pb$. Unlike v_2, v_3 and generally all odd harmonics origin from initial fluctuations. Moreover, v_2 and v_3 are not correlated. Hence both are needed for description of the system.

Hereby presented study was performed using the HYDJET++ Monte Carlo heavy-ion event generator. The model combines soft component based on parametrisation of relativistic hydrodynamics with jet routine based on PYQUEN. The two parts are independent, their interplay yields realistic shapes of flow distributions. HYDJET++ also contains vast table of resonances together with their possible decay channels, making investigation of final-state interactions on observed flow possible.

HYDJET++ was proved to yield good triangular distributions in Pb+Pb collisions at LHC energies. The combination of soft and hard component gives realistic shapes of v_3 distributions of the most abundant hadrons, namely protons, pions and kaons. Influence of resonance decays on triangular flow was also studied. Our calculations have shown that decays of heavy baryons and mesons affect the observed $v_3(p_T)$ distributions in a significant way. The products of such decays may carry larger flow and are more energetic, as their mothers also have larger p_T and stronger v_3. Decays of heavy resonances plays also an improtant role in the scaling picture. The number-of-constituent-quark-scaling was found to be broken at the LHC. Despite this fact, it presents still a useful tool to probe flow in greater depth.

The STAR Collaboration has recently presented the first preliminary data of triangular

flow of identified hadrons. Moreover, it was shown that v_3 in Au+Au at $\sqrt{s_{NN}} = 200$ GeV should scale as $v_3/n_q^{3/2}$. Our calculations in HYDJET++ seem to agree for v_3^p and v_3^π. However, the p_T dependent distribution for charged kaons does not match the released experimental data. Focusing on pions and protons, the calculations predict scaling as $v_3/n_q^{3/2}$, as suggested. The scaling is expected to be again result of resonance decays. There is, however, significantly less jets and they are softer compared to LHC, therefore the scaling is not destroyed. To track a possible source of the discrepancy between HYDJET++ calculations of kaon v_3 and the data presented by the STAR Collaboration, v_2 was also briefly inspected. Alas, the calculation do not match the PHENIX data. This issue needs to be investigated further in more depth. Right now, our results for RHIC energies are inconclusive.

Bibliography

[1] The Frontiers of Nuclear Science, 2007 NSAC Long Range Plan, http://www.sc.doe.gov/np/nsac/docs/Nuclear-Science.Low-Res.pdf, 03-04-2015.

[2] G. Odyniec, J. Phys. Conf. Ser. **455** (2013) 012037.

[3] M. Kliemant, R. Sahoo, T. Schuster and R. Stock, Lect. Notes Phys. **785** (2010) 23.

[4] T. Hirano *et al.*, Lect. Notes Phys. **785** (2010) 139.

[5] U. Heinz and R. Snellings, Annu. Rev. Nucl. Part. Sci. **63** (2013) 123.

[6] M. Luzum and P. Romatschke, Phys. Rev. Lett. **103** (2009) 262302.

[7] R. Vogt, *Ultrarelativistic Heavy-Ion Collisions*, Elsevier 2007, ISBN 978-0-444-52196-5.

[8] T. Dahms (CMS Collaboration), Nucl. Phys. A **910-911** (2013) 91.

[9] D. Tlustý (STAR Collaboration), Nucl. Phys. A **904-905** (2013) 639c.

[10] J. Adams *et al.* (STAR Collaboration), Phys. Rev. Lett. **91** (2003) 072304.

[11] Ch.-Y. Wong, *Introduction to High-Energy Heavy-Ion Collisions*, World Scientific 1994, ISBN 978-981-4506-85-4.

[12] L. Adamczyk *et al.* (STAR Collaboration), Phys. Rev. Lett. **113** (2014) 022301.

[13] A. Adare (PHENIX Collaboration), Phys. Rev. C **81** (2010) 034911.

[14] M. Wilde (ALICE Collaboration), Nucl. Phys. A**904-905** (2013) 573c.

[15] S. Voloshin and Y. Zhang, Z. Phys. C **70** (1996) 665.

[16] R. Snellings, New J. Phys. **13** (2011) 055008.

[17] B. Alver and G. Roland, Phys. Rev. C **81** (2010) 054905.

[18] K. Aamodt *et al.* (ALICE Collaboration), Phys. Rev. Lett. **105** (2010) 252302.

[19] P. Steinberg, New J. Phys. 14 (2012) 035006.

[20] J. Adams *et al.* (STAR Collaboration), Phys. Rev. Lett. **92** (2004) 062301.

[21] X. Sun (for STAR Collaboration), J. Phys.: Conf. Ser. **535** (2014) 012005.

[22] A. Adare *et al.* (PHENIX Collaboration), Phys. Rev. Lett **98** (2007) 162301.

[23] K. Aamodt *et al.* (ALICE Collaboration), Phys. Rev. Lett **107** (2011) 032301.

[24] M. Krzewicki (for ALICE Collaboration), J. Phys. G **38** (2011) 124047.

[25] S. Chatrchyan *et al.* (CMS Collaboration), Phys. Rev. C **89** (2014) 044906.

[26] G. Aad *et al.* (ATLAS Collaboration), Phys.Rev. C **86** (2012) 014907.

[27] A. Adare *et al.* (PHENIX Collaboration), Phys. Rev.Lett. **105** (2010) 062301.

[28] X. Sun (STAR Collaboration), Nucl. Phys. A **931** (2014) 1194.

[29] L. X. Han, G. L. Ma, Y. G. Ma, X. Z. Cai, J. H. Chen, S. Zhang and C. Zhong, Phys. Rev. C **84** (2011) 064907.

[30] B. Abelev *et al.* (ALICE Collaboration), Phys. Lett. B **726** (2013) 164.

[31] *The Abel computer cluster*, http://www.uio.no/english/services/it/research/hpc/abel/, 16-03-2015.

[32] I. P. Lokhtin *et al.*, Comp. Phys. Comm. **180** (2009) 779–799.

[33] *HYDJET++ event generator*, `http://lokhtin.web.cern.ch/lokhtin/hydjet++/`, March 2014.

[34] Private communication with Ludmila Malinina, 16-04-2014.

[35] B. Abelev *et al.* (ALICE Collaboration), Phys. Rev. C **88** (2013) 044910.

[36] B. Back *et al.* (PHOBOS Collaboration), Phys. Rev. Lett **91** (2003) 052303.

[37] B. Abelev *et al.* (STAR Collaboration), Phys. Rev. Lett. **97** (2006) 152301.

[38] G. Eyyubova *et al.*, Phys. Rev. C **80** (2009) 064907.

[39] L. Bravina *et al.*, Phys. Rev. C **87** (2013) 034901.

[40] L. Bravina *et al.*, Eur. Phys. J. C **74** (2014) 2807.

[41] J. Beringer *et al.* (Particle Data Group), Phys. Rev. D **86** (2012) 010001.

Appendix A

Poster and proceedings from Bormio 2015

Results of our study were presented at the 53$^{\text{rd}}$ International Winter Meeting on Nuclear Physics in Bormio, 26-30 January 2015. Proceedings was accepted for publication at the Proceedings of Science:

Jana Crkovská, Larissa Bravina, Evgeny Zabrodin and Gyulnara Eyyubova, *Simulation of Hadronic Triangular Flow in Relativistic Heavy Ion Collisions*, PoS (Bormio2015) 007, http://pos.sissa.it/archive/conferences/238/007/Bormio2015_007.pdf

Triangular flow in heavy-ion collisions

Jana Crkovská[1]*, Larissa Bravina[2], Evgeny Zabrodin[2,3], Gyulnara Eyyubova[1,3]

[1]Faculty of Nuclear Sciences and Physical Engineering, Czech Technical University in Prague, Czech Republic
[2]Faculty of Mathematics and Natural Sciences, University of Oslo, Norway
[3]Skobeltsyn Institute of Nuclear Physics, Lomonosov Moscow State University, Russia

Abstract

The hadronic collective flow was found to be one of the most pronounced signatures of the QGP. Hydrodynamical calculations have shown that the spatial anisotropy of the initial overlap zone of the nucleus-nucleus collisions is transferred into the final state momentum anisotropic flow. The invariant differential cross section can be expanded into a Fourier series over the azimuthal angle, with flow harmonics figuring as Fourier coefficients. At high energies the elliptic flow, defined by the second Fourier coefficient v_2, dominates the Fourier expansion for semi-peripheral and peripheral collisions. In central collisions the contribution of the third component v_3 becomes more pronounced due to the spatial initial state fluctuations.

Study of triangular flow in Pb+Pb collisions at $\sqrt{s_{NN}}$ = 2.76 TeV and in Au+Au collisions at $\sqrt{s_{NN}}$ = 200 GeV was performed using HYDJET++ Monte Carlo model [1]. The model enables study of influence of final-state interactions on flow of created hadrons. The interplay between jet physics and soft hydrodynamics, as well as the influence of the resonance decays on the triangular flow in AA collisions at RHIC and LHC were studied.

Anisotropic flow of particles

The invariant differential cross section can be expanded into a Fourier series w. r. t. reaction plane:

$$E\frac{d^3N}{d^3p} = \frac{1}{2\pi\,p_T dp_T dy}\frac{d^2N}{}\left(1 + \sum_{n=1}^{\infty} 2v_n \cos\left(n\phi - n\Psi_R\right)\right)$$

$$v_n = \langle\cos\left(n\phi - n\Psi_R\right)\rangle$$
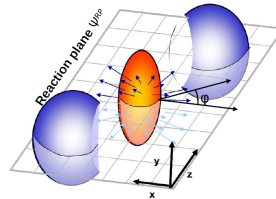
The initial spatial anisotropy of the system gives rise to even harmonics, from which the elliptic flow v_2 is of great importance. As the system evolves, the pressure gradients inside the fireball drive the system towards spatial symmetry, thus creating anisotropy in the momenta of the outcoming particles. Once the system has acquired symmetric shape, the evolution ceases. Hence the flow development takes place at early stage of the collision, when the quark-gluon plasma is still present.

Number-of-constituent-quark scaling (NCQ) was revealed to be a prominent feature of elliptic flow at RHIC [2]. Such observation suggests that flow is formed at partonic level. However, NCQ scaling is broken at LHC energies.

HYDJET++

HYDJET++ is a Monte Carlo heavy-ion event generator [1]. It acts as a superposition of a soft hydro-part and a hard-part containing jets, both of which are treated independently.

Soft-part: hadrons generated on freeze-out hypersurface described by relativistic hydrodynamics

Hard-part: binary collisions at b from Glauber model, parton further evolved only if $p_T > p_T^{min}$
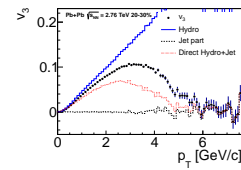
The hydro-driven part produces the growth of the distribution and mass ordering while the fall-off at higher p_T and branch crossing occurs due to jet-quenching.

Triangular flow at LHC

Resonance decays increase the magnitude of the flow distribution and shift the maximum to higher p_T. Lightest particles (pions) are affected more than heavier baryons such as Λ.
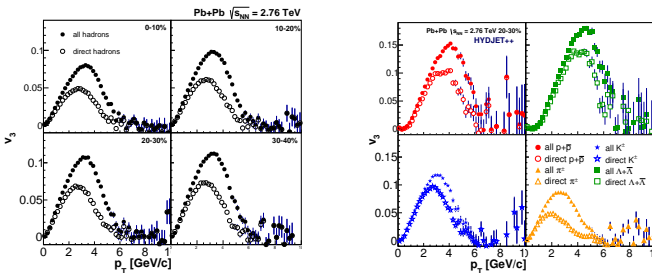
Preliminary results from LHC suggest that the NCQ scaling for v_3 is broken [3]. Scaling $v_3/n_q(kE_T/n_q)$ and its changing due to resonance decays has been studied. According to our HYDJET++ calculations, the scaling seems to be broken indeed. However the decays of resonances drive the distributions towards scaling behaviour.
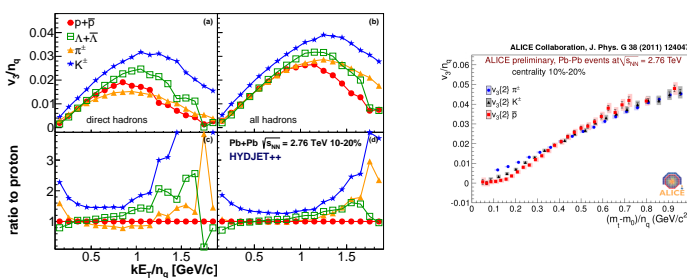
Triangular flow at RHIC

HYDJET++ gives a fairly good description of STAR data [4]. Branching is less pronounced than at LHC energies. HYDJET++ however yields higher flow of kaon that reported by STAR, this needs to be studied further in detail.
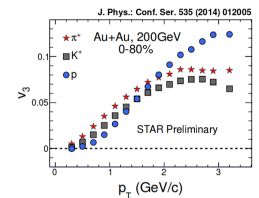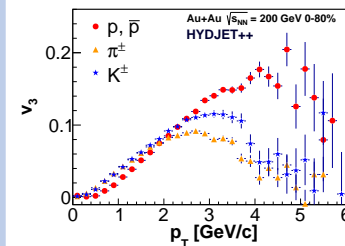
STAR have recently announced preliminary results showing the NCQ scaling behaviour as $v_3/n_q^{3/2}(kE_T/n_q)$ [4]. As in the case of LHC, decays of resonances drive flow towards fulfilment of scaling behaviour.

Acknowledgement
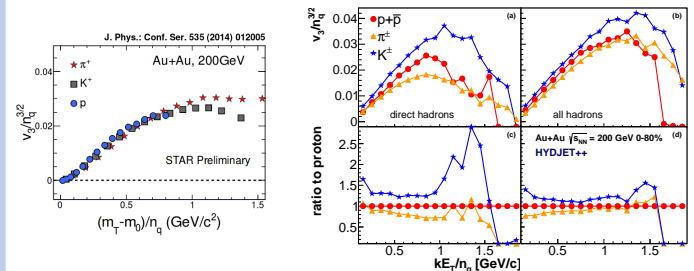
Conclusions

It was shown that HYDJET++ provides a good description of triangular flow in collisions of heavy ion. The shape of distributions is successfully described by the interplay of hydrodynamics and jets.

Effects of resonance decays on triangular flow were studied. These decays influence shape of distributions of observed hadrons by increasing the magnitude and by shift of the maximum to higher p_T. Resonances drive flow towards NCQ scaling fulfilment. Role of jets needs to be studied in more detail.

References

[1] I. P. Lokhtin et al., Comp. Phys. Comm. 180 (2009) 779799.
[2] A. Adare et al. (PHENIX Collaboration), Phys. Rev. Lett 98 (2007) 162301.
[3] M. Krzewicki (for ALICE Collaboration), J. Phys. G 38 (2011) 124047.
[4] X. Sun (for STAR Collaboration), J. Phys.: Conf. Ser. 535 (2014) 012005.

Simulation of Hadronic Triangular Flow in Heavy-Ion Collisions

Jana Crkovská[*a], **Larissa Bravina**[b], **Gyulnara Eyyubova**[ac] **and Evgeny Zabrodin**[bc]

[a] *Faculty of Nuclear Sciences and Physical Engineering, Czech Technical University in Prague,*
Břehová 7, 115 19 Prague, Czech Republic

[b] *Department of Physics, University of Oslo, P. O. Box 1048 Blindern, N-0316, Oslo, Norway*

[c] *Skobeltsyn Institute of Nuclear Physics, Lomonosov Moscow State University, GSP-1, Moscow*
119991, Russian Federation

E-mail: crkovjan@fjfi.cvut.cz,

Study of triangular flow in Pb+Pb collisions at $\sqrt{s_{NN}} = 2.76$ TeV and in Au+Au collisions at $\sqrt{s_{NN}} = 200$ GeV was performed using HYDJET++ Monte Carlo model. The model combines description of hard scatterings in hot and dense partonic medium with the treatment of soft processes represented by parametrized hydrodynamics. The interplay between jet production and hydrodynamics, as well as the influence of the resonance decays on the triangular flow in AA collisions at RHIC and LHC were studied. It was found that the decays of resonances increase the magnitude of the $v_3(p_T)$ distribution at $p_T \geq 1$ GeV$/c$ and shift its maximum to higher transverse momenta. Resonances also drive the v_3 toward the NCQ scaling fulfilment, whereas jets cause the scaling violation at the LHC.

---

[*]Speaker.

---

1. Anisotropic flow of particles

The hadronic collective flow is one of the most pronounced signatures of QGP produced in ultrarelativistic heavy ion collisions at the RHIC and at the LHC. Hydrodynamical calculations have shown that the spatial anisotropy of the initial overlap zone of the nucleus-nucleus collisions is transferred into the final state momentum anisotropic flow. The invariant differential cross section can be expanded into a Fourier series w. r. t. reaction plane Ψ_R:

$$E\frac{\mathrm{d}^3N}{\mathrm{d}^3p} = \frac{1}{2\pi}\frac{\mathrm{d}^2N}{p_T\mathrm{d}p_T\mathrm{d}y}\left(1+\sum_{n=1}^{\infty}2v_n\cos\left(n\varphi-n\Psi_R\right)\right)$$

$$v_n = \langle\cos\left(n\phi-n\Psi_R\right)\rangle$$

where p_T stands for transverse momentum, y denotes rapidity and φ represents azimuthal angle of the particle [1]. At high energies the elliptic flow, defined as the second Fourier coefficient v_2, dominates the Fourier expansion for semi-peripheral and peripheral collisions. With collisions centrality, the contribution of the third Fourier coefficient, triangular flow v_3, becomes more pronounced due to the spatial initial state fluctuations.

Measurement of flow can, among other, yield information about the characteristics of medium created in collisions. Elliptic flow measured at RHIC suggests creation of ideal liquid with very low viscosity [2]. Triangular flow can unveil new information in such measurements as it enables comparison of multiple parameters depending on viscosity [3].

Number-of-constituent-quark scaling (NCQ) is a prominent feature of elliptic flow at RHIC energies [4]. In other words, all quarks at given p_T carry the same flow independently on the system they are bound in, suggesting that flow is formed at partonic level. Because jets are significantly more abundant and energetic at the LHC than at the RHIC, NCQ scaling is broken at LHC energies. Recent studies have shown that triangular flow scales at the RHIC as $v_3/n_q^{3/2}$ [5], see Fig. 1a. The ALICE experiment investigated scaling v_3/n_q [6] as shown in Fig. 1b. As in the case of v_2, the scaling is broken.

2. HYDJET++

HYDJET++ [7] is a Monte Carlo heavy-ion event generator composed of two independent parts. The soft part of the model is represented by parametrized relativistic hydrodynamics, describing a transition from hot and dense lump of partonic substance to a freeze-out hypersurface on which the partons are generated. The hard part containing jets deals with binary collisions at given impact parameter b. Partons with transverse momenta $p_T > p_T^{min}$ are further evolved further medium, while the rest are hadronised and included in the soft component.

The interplay of the two parts yields realistic shapes of flow distributions. The soft part of distributions is dominated by the hydro-driven soft component, resulting in rise of the distribution and observed mass ordering. The subsequent fall-off resulting in crossing of meson and baryon branches is caused by jets being gradually more prominent with higher p_T.

(a)   (b)
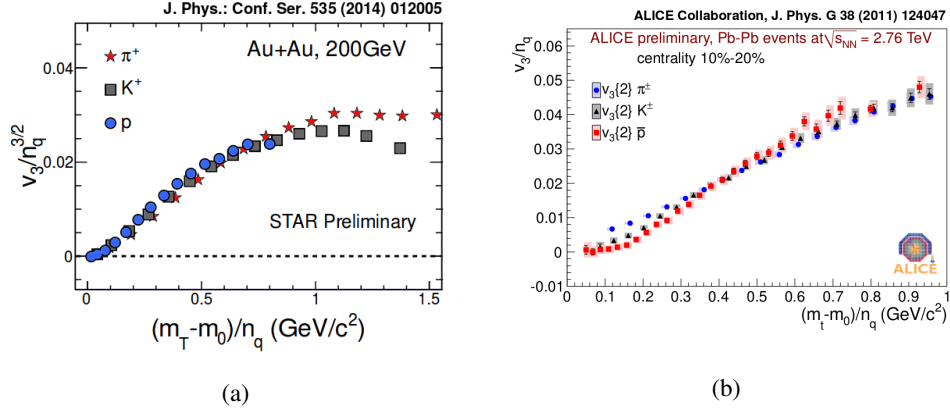
Figure 1: (a) Number-of-constituent-quark scaling $v_3/n_q^{3/2}$ vs (kE_T/n_q) in minimum bias Au+Au collisions at $\sqrt{s_{NN}} = 200$ GeV [5]. (b) v_3/n_q vs (kE_T/n_q) in Pb+Pb collision at $\sqrt{s_{NN}} = 2.76$ TeV at centrality 10-20% [6].

3. Triangular flow at the LHC

We have studied the effect of final-state interactions on triangular flow in Pb+Pb collision at $\sqrt{s_{NN}} = 2.76$ TeV. Comparison between the flow distributions of direct hadrons, i. e. hadrons produced directly from the medium, and all hadrons recorded in the event is shown in Fig. 2a.

(a)   (b)
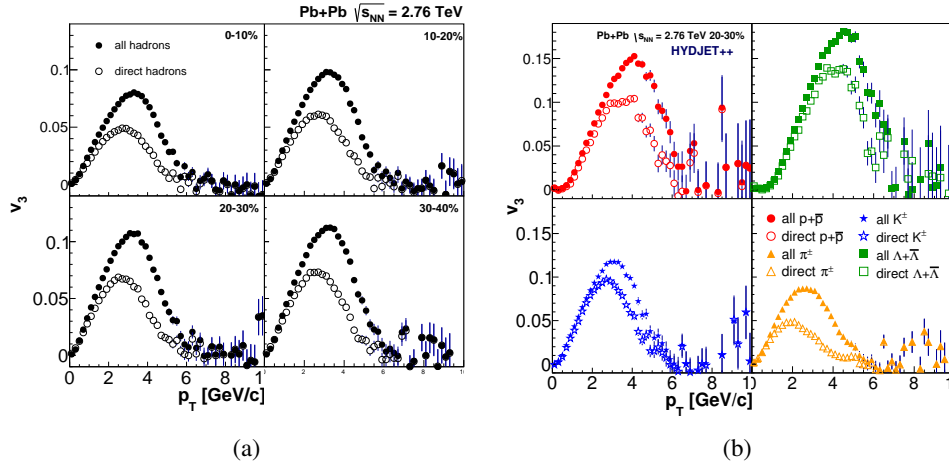
Figure 2: Pb+Pb collision at $\sqrt{s_{NN}} = 2.76$ TeV in HYDJET++. (a) Triangular flow for all hadrons (full circles) and for directly produced hadrons (open circles). (b) Triangular flow of protons (red circles), lambdas (green squares), charged kaons (blue stars) and charged pions (yellow triangles). Full symbols denote flow of all particles produced in the event, open symbols show flow of direct particles only.

HYDJET++ describes the LHC data quite successfully [8]. Triangular flow of charged parti-

cles changes rather weakly with centrality, which is in agreement with experimental data [3]. The magnitude of flow in maximum is significantly increased by decays of resonances, the maximum is also shifted into higher p_T by about 10% of the original value. Fig 2b portrays the comparison of direct and total flow distribution at 20-30% centrality window for different hadron species separately, namely protons, lambdas, kaons and pions. The effect of resonance decays is strongest in case of the lightest particles, i. e. pions, while heavier particles such as lambdas are only marginally affected.

Preliminary results from LHC suggest that the NCQ scaling for v_3 is broken [6]. Scaling $v_3/n_q(kE_T/n_q)$ and its changing due to resonance decays has been studied. According to HYDJET++ calculations, shown in Fig. 3, the scaling seems to be broken indeed. However the decays of resonances drive the distributions towards scaling fulfilment.
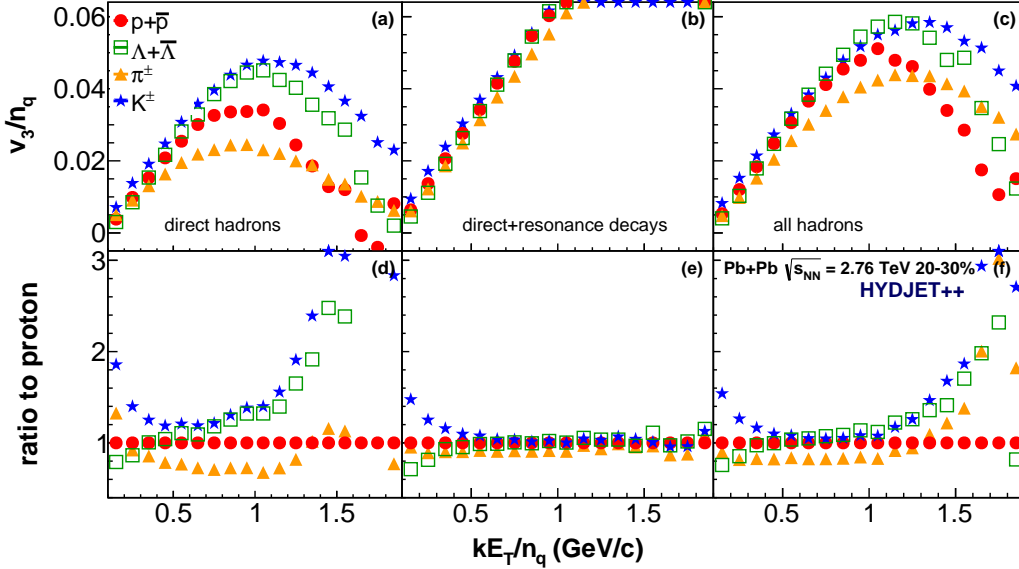
Figure 3: v_3/n_q vs kE_T/n_q in Pb+Pb collision at $\sqrt{s_{NN}} = 2.76$ TeV in HYDJET++. (a) Direct hydro+jets , (b) direct+from decays of resonances and (c) total distributions for protons (red circles), lambdas (green open squares), charged kaons (blue stars) and charged pions (yellow triangles). (d), (e) and (f) show the respective three distributions divided by the corresponding proton distribution.

4. Triangular flow at the RHIC

Triangular flow at RHIC energies has been also investigated. v_3 of protons, charged kaons and charged pions in Au+Au collisions at $\sqrt{s_{NN}} = 200$ GeV is displayed in Fig. 4. While the proton and pion distributions agree rather well with STAR data [5], the kaons manifest much stronger flow in HYDJET++. Where STAR saw blurring of the meson and baryon branch, HYDJET++ shows a strict branching.

This also affects the results for NCQ scaling observation, see Fig. 5. As in the case of LHC, the direct distributions at RHIC display no scaling behaviour (a, c). Only by counting in the decays of resonances, one obtains a reasonable scaling scenario (b, d).
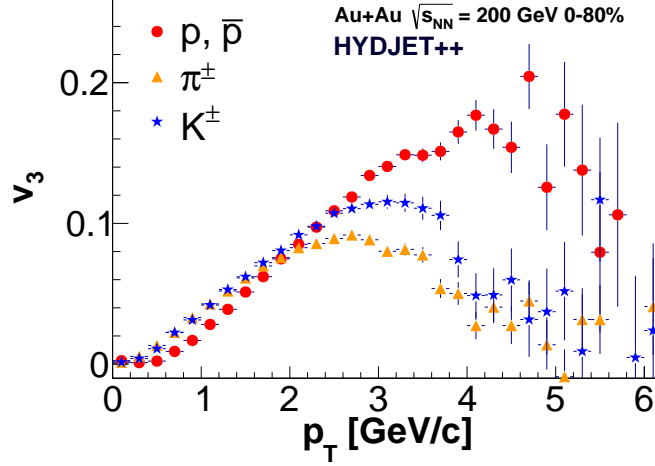
Figure 4: Triangular flow distributions $v_3(p_T)$ for protons (red circles), charged kaons (blue stars) and charged pions (yellow triangles) in Au+Au collisions at $\sqrt{s_{NN}} = 200$ GeV in HYDJET++.

5. Conclusions

HYDJET++ provides a good description of triangular flow in relativistic heavy-ion collisions. Resulting shape of distributions comes naturally from the interplay of hydrodynamics and jets. The model enables study of final-state-interaction effects on flow distributions.

Influence of resonance decays on triangular flow at LHC and at RHIC energies was investigated. Decays change significantly the shape of the distribution by increasing the amplitude in the maximum and by its shift to higher p_T region. Resonances also drive flow towards NCQ scaling behaviour. Scaling is still broken at LHC energies, this effect is attributed to the energetic jets

Acknowledgement
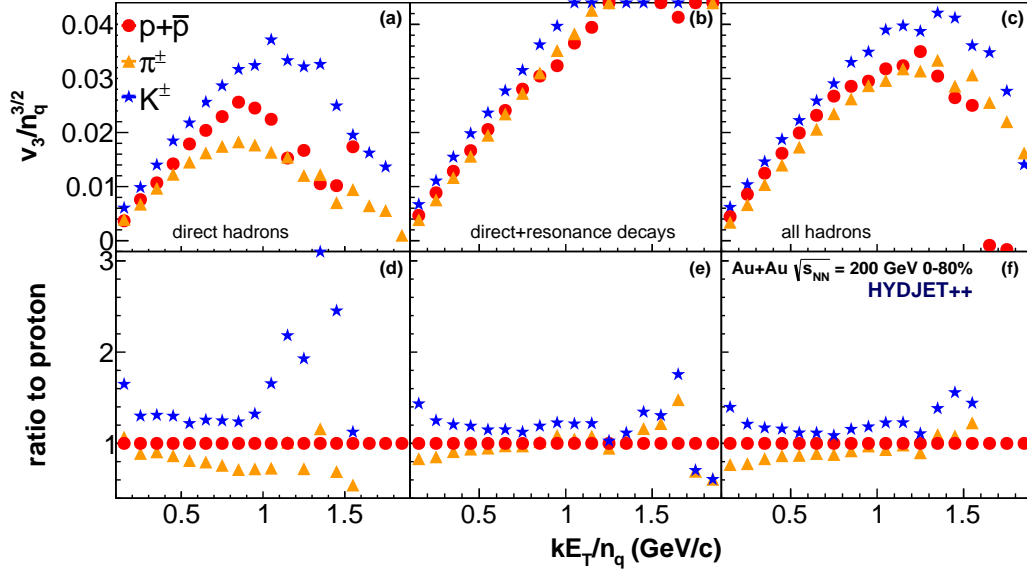
Figure 5: v_3/n_q vs kE_T/n_q in Au+Au collision at $\sqrt{s_{NN}} = 200$ GeV in HYDJET++. (a) Direct hydro+jets , (b) direct+from decays of resonances and (c) total distributions for protons (red circles), kaons (blue stars) and pions (yellow triangles). (d), (e) and (f) show the respective three distributions divided by the corresponding proton distribution.

References

[1] S. Voloshin and Y. Zhang, Z. Phys. C 70 (1996) 665.

[2] M. Gyulassy and L. McLerran, Nucl. Phys. A 750 (2005) 30.

[3] K. Aamodt *et al.* (ALICE Collaboration), Phys. Rev. Lett. 107 (2011) 032301.

[4] A. Adare *et al.* (PHENIX Collaboration), Phys. Rev. Lett. 98 (2007) 162301.

[5] X. Sun (for STAR Collaboration), J. Phys.: Conf. Ser. 535 (2014) 012005.

[6] M. Krzewicki (for ALICE Collaboration), J. Phys. G 38 (2011) 124047.

[7] I. P. Lokhtin *et al.*, Comp. Phys. Comm. 180 (2009) 779.

[8] L. Bravina *et al.* Eur. Phys. J. C74 (2014) 2807.

Appendix B

Proceedings from the 18$^{\text{th}}$ Conference of Czech and Slovak Physicists

Results of our study were presented at the 18$^{\text{th}}$ Conference of Czech and Slovak Physicists. Proceedings was accepted for publication at the EPJ Web of Conferences.

Influence of resonance decays on triangular flow in heavy-ion collisions

Jana Crkovská[1], Larissa Bravina[2], and Evgeny Zabrodin[2,3]

[1]*Faculty of Nuclear Sciences and Physical Engineering, Czech Technical University in Prague, Břehová 7, Prague 110 00, Czech Republic, crkovjan@fjfi.cvut.cz*
[2]*Department of Physics, University of Oslo, P. O. Box 1048 Blindern, N-0316, Oslo, Norway*
[3]*Skobeltsyn Institute of Nuclear Physics, Lomonosov Moscow State University, Leninskie Gory, GSP-1, Moscow 119991, Russian Federation*

Abstract. Anisotropic flow in relativistic collisions of heavy-ions yields important information about the state of the hot and dense matter created in the reactions. Study of triangular flow in Pb+Pb interactions at LHC was performed within Monte Carlo HYDJET++ model. HYDJET++ combines both parametrized hydrodynamics for soft p_T particle spectra and microscopic jet quenching generator for hard p_T spectra, giving a realistic prediction for vast number of hadron species. The model also enables study of influence of final-state interactions on flow of created hadrons. Triangular flow patterns of pions, kaons and protons were studied at different centralities. Scaling of triangular flow with number of constituent quarks is discussed.

1 Introduction

Collective flow of particles can yield valuable information about the hot and dense medium created in relativistic nucleus-nucleus collisions, known as quark-gluon plasma (QGP). The initial anisotropy of the overlap region and the subsequent expansion of the fireball after the collision due to the pressure gradients inside give rise to momentum anisotropy of outcoming particles. The azimuthal distribution of detected particles with respect to reaction plane Ψ_R can be expanded into a Fourier series

$$\frac{\mathrm{d}N}{\mathrm{d}\varphi} = \frac{N}{2\pi}\left[1 + 2\sum v_n \cos\left(n(\varphi - \Psi_R)\right)\right], \quad (1)$$

with the Fourier coefficients describing high flow harmonics

$$v_n = \langle\cos\left(n(\varphi - \Psi_R)\right)\rangle \quad (2)$$

and bear the name of directed, elliptic and triangular flow for v_1, v_2 and v_3 respectively. Measuring the magnitude of the flow coefficients can yield information about the state of the medium produced immediately after the initial scattering. Elliptic flow presented the dominant contribution to anisotropic flow in semi-peripheral and peripheral interactions. However with energies such as at LHC, the higher coefficients grow significantly and become dominant at small impact parameters. Results from LHC suggest that in central collisions the main part of the anisotropic flow originates from the triangular flow [1].

A prominent feature of elliptic flow is the number-of-constituent-quarks scaling (NCQ), first observed at RHIC [2]. The elliptic flow for identified particles scales as $v_2/n_q(kE_T/n_q)$. Such behaviour implies formation of flow on partonic level, when the QGP is still present, and favours coalescence formation scenario. Preliminary results from STAR experiment suggest that v_3 scales as $v_3/n_q^{3/2}(kE_T/n_q)$ [3].

2 HYDJET++

HYDJET++ [4] stands for HYDrodynamics with JETs and is a Monte Carlo heavy-ion event generator. It is a superposition of hydrodynamical part and jet part. These are treated independently. Among the advantages of this model is the possibility to study separately hydrodynamical behaviour and influence of jet quenching, its efficiency, its ability to reproduce realistic shapes of distributions and that it includes a vast table of resonances.
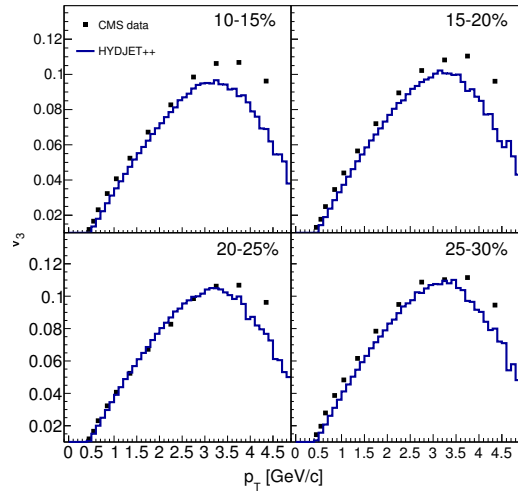
Figure 1. Triangular flow of charged particles in Pb+Pb at $\sqrt{s_{NN}} = 2.76$ TeV. Histograms are HYDJET++ calculations, squares are CMS data [6].

3 Triangular flow at LHC

Hereby we studied the influence of decays of the resonances on triangular flow at LHC energies. HYDJET++ was tuned to give realistic shapes of v_2 and v_3 distributions [5]. In Figure 1 the v_3-distributions

over transverse momentum p_T for charged particles (protons, pions and kaons) in Pb+Pb collisions at $\sqrt{s_{NN}} = 2.76$ TeV obtained with HYDJET++ (histogram) are compared with CMS data [6]. The model provides a particulary good description of data in soft p_T region. The overall shape of the distribution corresponds to the trend observed in experiment as advertised.
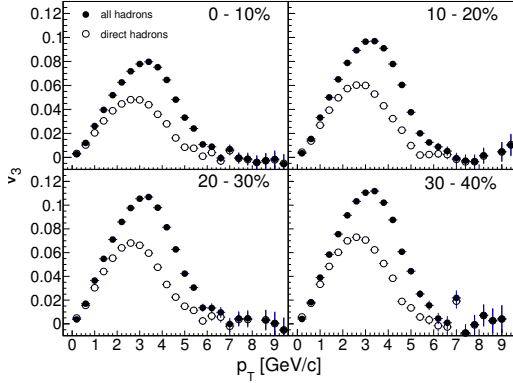
Figure 2. Triangular flow distribution $v_3(p_T)$ for all charged particles (full circles) and direct charged particles (open circles) in Pb+Pb at $\sqrt{s_{NN}} = 2.76$ TeV.

Figure 2 shows the triangular flow $v_3(p_T)$ of all charged particles (full circles) and of only directly produced particles (open circles) in Pb+Pb at $\sqrt{s_{NN}} = 2.76$ TeV in four centrality bins. The effect of resonance decays is significant both in magnitude and in position of the maximum of distributions. The maximum of the distribution is shifted to higher p_T of about 10% while the amplitude difference is about 40% in all centrality bins.

NCQ scaling of triangular flow at LHC was also studied. We considered the v_3 to scale as $v_3/n_q^{3/2}$. Results for protons, kaons and pions are shown in Figure 3 (a, b) for all hadrons and directly produced hadrons respectively. Plots (c, d) show the distributions (a, b) respectively divided by the corresponding distribution for proton. Proton and pion distributions seem to follow the scaling for low p_T, however the kaon distribution deviates by more than 50%. For directly produced kaons the deviation from scaling is more significant, while protons and pions are still well scaled. The conclusion remains the same as for elliptic flow[7]: NCQ scaling is violated at LHC, but resonance decays drive the corresponding ratios v_2/n_q and $v_3/n_q^{2/3}$ towards the scaling fulfilment. The role of jet quenching in the violation of the NCQ scaling still needs to be clarified.

4 Conclusion

We performed a study of the effect of resonance decays on the triangular flow in Pb+Pb collisions within the HYDJET++ framework. The model provides a fair description of v_3 with centrality. It was found that resonances influence significantly the shape of flow distributions: for v_3 we observed in maximum a shift of about 10% to higher p_T and growth of about 40% in amplitude. It is vital to further study the flow of mother and daughter particles as well as influence of jets to better understand the dynamics of the system.
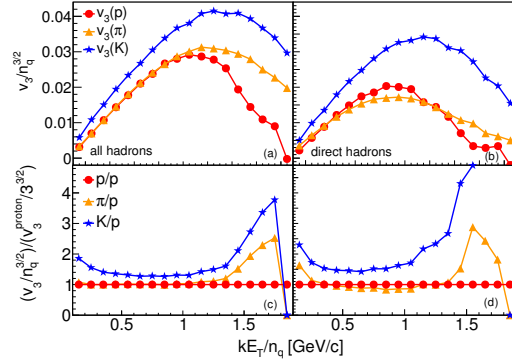
Figure 3. Number-of-constituent-quarks scaling for triangular flow in Pb+Pb at $\sqrt{s_{NN}} = 2.76$ TeV. Distributions for all protons (circles), pions (triangles) and kaons (stars) are shown in (a), for direct particles in (b). The distributions of all particles divided by the proton distribution are depicted in (c), (d) shows the same for direct particles.

Acknowledgement

References

[1] Aamodt, K. *et al.* (ALICE Collaboration), Phys. Rev. Lett 107 (2011) 032301.

[2] A. Adare *et al.* (PHENIX Collaboration), Phys. Rev. Lett 98 (2007) 162301.

[3] Sun, X. (for STAR Collaboration), J. Phys.: Conf. Ser. 535 (2014) 012005.

[4] Lokhtin, I. P. *et al.*, Comp. Phys. Comm. 180 (2009) 779–799.

[5] Bravina, L. V. *et al.*, Eur. Phys. J. C 74 (2014) 2807.

[6] Chatrchyan, S. *et al.* (CMS Collaboration), Phys. Rev. C 87 (2013) 014902.

[7] Eyyubova, G. *et al.* Phys. Rev. C 80 (2009) 064907.

Appendix C

Proceedings from the ICNFP 2014

Results of our study were presented at the 3rd International Conference on New Frontiers in Physics 2014. Proceedings was accepted for publication at the EPJ Web of Conferences.

Influence of resonance decays on triangular flow in heavy-ion collisions

J. Crkovská[1,2, a], L. V. Bravina[2], G .Kh. Eyyubova[1,3], and E. E. Zabrodin[2,3]

[1]*Faculty of Nuclear Sciences and Physical Engineering, Czech Technical University in Prague, Břehová 7, 110 00 Prague, Czech Republic*
[2]*Department of Physics, University of Oslo, P. O. Box 1048 Blindern, N-0316, Oslo, Norway*
[3]*Skobeltsyn Institute of Nuclear Physics, Lomonosov Moscow State University, Leninskie Gory, GSP-1, Moscow 119991, Russian Federation*

Abstract. Anisotropic flow in relativistic collisions of heavy-ions yields important information about the state of the hot and dense matter created in the collision. Study of triangular flow in Pb+Pb collisions at LHC was performed using HYDJET++ Monte Carlo generator. HYDJET++ combines both hydrodynamics-driven soft part together with hard jet-part, giving a realistic prediction for vast number of hadron species. The model also enables study of influence of final-state interactions on flow of created hadrons. Triangular flow patterns of pions, kaons and protons were studied. We found that resonance decays influence significantly the shape of the distributions.

1 Introduction

Relativistic heavy-ion collisions present a unique tool for study of matter under extreme conditions. The high temperatures and energy densities give rise to new state of matter known as the quark-gluon plasma (QGP). The thermalised hot and dense matter does expand and cool down until it reaches critical temperature and goes through a phase transition into a hadronic matter. The freeze-out does occur very shortly after the initial collisions, in order of $\sim$ 10 ps. Hence the QGP cannot be detected directly, one would need some signatures that would permit further studies of this new exotic phase of matter.

Flow is a collective motion of matter created in collision, created by the pressure gradient inside the fireball, thus giving additional boost to the out-coming particles. The azimuthal distribution of created particles emitted at angle ϕ with respect to reaction plane Ψ_R can be expanded into a Fourier series as

$$\frac{\mathrm{d}N}{\mathrm{d}\varphi} = \frac{N}{2\pi}\left[1 + 2\sum v_n \cos\left(n(\varphi - \Psi_R)\right)\right],\tag{1}$$

where the Fourier coefficients are in a form

$$v_n = \langle\cos\left[n(\phi - \Psi_R)\right]\rangle.\tag{2}$$

---

a. e-mail: crkovjan@fjfi.cvut.cz

The elliptic flow v_2 gives the dominant contribution to anisotropic flow in peripheral and semi-peripheral collisions. v_2 arises from the asymmetry of the overlap zone. As the spatially anisotropic fireball evolves, it resumes spatial symmetry, thus giving rise to momentum anisotropy of out-coming particles. Hence it is a self-quenching phenomenon which takes place early after the collision when the QGP is still present. However the actual overlap zone fluctuates event-by-event around the geometrical zone. Triangular flow v_3 originates from such initial fluctuations.

Number-of-constituent-quarks (NCQ) scaling is a prominent feature of elliptic flow, first observed in 2007 at RHIC [2]. Elliptic flow of identified hadron species was divided by number of quarks inside of each species and ploted as a function of transverse kinetic energy. The resulting distributions were of identical shape for all studied species. Recent results from STAR suggest that v_3 scales as $v_3/n_q^{3/2}(kE_T/n_q)$ [3].

2 HYDJET++

HYDJET++ [4] stands for HYDrodynamics with JETs and is a Monte Carlo heavy-ion event generator. It is a superposition of hydrodynamical part and jet part. Each part is treated independently. Among the advantages of this model is its efficiency, its ability to reproduce realistic shapes of distributions and that it includes a vast table of resonances.

In the soft part, the hadrons are generated on freeze-out hyper-surface described by a parametrisation of relativistic hydrodynamics with given initial conditions and equation of state. The jets are generated from binary collisions at given impact parameter b from Glauber model. Only partons fulfilling the condition $p_T > p_T^{min}$ are further evolved. Those with transverse momentum lower than the threshold value are thermalised and their hadronisation products are included in the soft component.

The elliptic flow is generated through spatial anisotropy $\varepsilon(b)$ and momentum anisotropy $\delta(b)$ as follows:

$$\varepsilon(b) = \frac{R_y^2 - R_x^2}{R_y^2 + R_x^2}$$

$$\frac{u^y}{u^x} = \sqrt{\frac{1 - \delta(b)}{1 + \delta(b)}} \tan \phi \tag{3}$$

where R_x and R_y are the projection of the fireball radius onto the x-direction and y-direction respectively and $u^{x,y}$ is the fluid velocity in corresponding direction. The anisotropy parameters $\varepsilon(b)$ and $\delta(b)$ were obtained by fitting the experimental data.

To obtain triangular flow, the radius of the freeze-out surface has to be modified using an additional triangularity parameter $\varepsilon_3(b)$ as

$$R(b, \phi) = R_f(b) \frac{\sqrt{1 - \varepsilon^2(b)}}{\sqrt{1 - \varepsilon(b) \cos 2\phi}} \{1 + \varepsilon_3(b) \cos[3(\phi - \Psi_3)]\}. \tag{4}$$

The axis Ψ_3 is generated randomly w.r.t. Ψ_2, therefore, elliptic and triangular flows are uncorrelated.

3 Triangular flow at LHC

We performed a study of the influence of decays of the resonances on triangular flow at LHC energies. HYDJET++ was tuned to give realistic shapes of v_2 and v_3 distributions [5]. In Fig. 1 the generated v_3 distribution for charged particles (protons, pions and kaons) in Pb+Pb collisions at
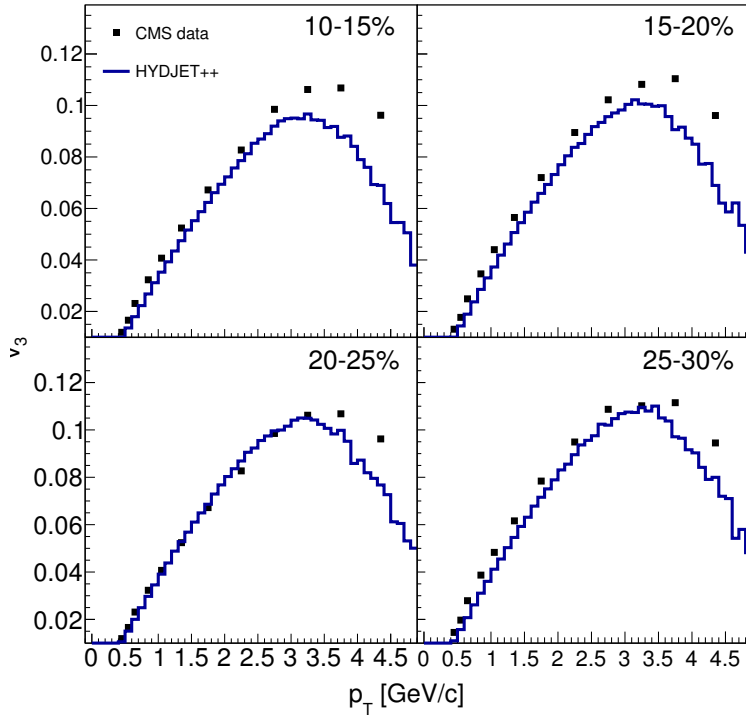
Figure 1. Triangular flow of charged particles in Pb+Pb at $\sqrt{s_{NN}}$ = 2.76 TeV. Histograms are HYDJET++ calculations, squares are CMS data [6].

$\sqrt{s_{NN}}$ = 2.76 TeV is compared with CMS data [6]. The model provides a particularly good description of data in softer region. The overall shape of the distribution corresponds to the trend observed in experiment.

Transverse momentum distributions of triangular flow $v_3(p_T)$ are shown in Fig. 2. Black dots show triangular flow distribution for all charged particles calculated with HYDJET++. Blue solid line shows flow obtained from the hydro-part of the model. The observed rise in flow is due to hydrodynamics, however already at low p_T, the real distribution starts to deviate from the hydro-calculation. At high p_T the majority of particles are produced from jets, which carry little flow (see black dashed line), thus explaining the fall in the distribution. The distribution for direct charged particles (red dashed line) follows a pattern similar to all charged particles.

Upper plot in Fig 3 shows calculation of $v_3(p_T)$ for protons, pions and kaons. The patterns show a meson-baryon branching in soft region and branch-crossing at higher p_T which is indeed observed experimentally. Mass ordering is also apparent, as the lightest particles resist to the push from medium the least. Bottom plot pictures $v_3(p_T)$ for protons, pions and kaons coming from hydrodynamics within HYDJET++. Mass-ordering and branching can be explained by hydrodynamics, however to fully describe the shape of the total distribution and the branch-crossing, another mechanism needs to be taken into account.

Fig. 4 shows $v_3(p_T)$ for charged particles in Pb+Pb at $\sqrt{s_{NN}}$ = 2.76 TeV, calculated with HYDJET++. Calculations were carried in 4 centrality bins within the range of $0 - 40\%$. Full circles represent flow of all charged particles while open circles show flow of direct charged particles. The effect of resonance decays is significant both in magnitude and in position of the maximum of distributions. The maximum of the distribution is shifted to higher p_T of about 10% while the difference of amplitude is about 40% in all centrality bins.
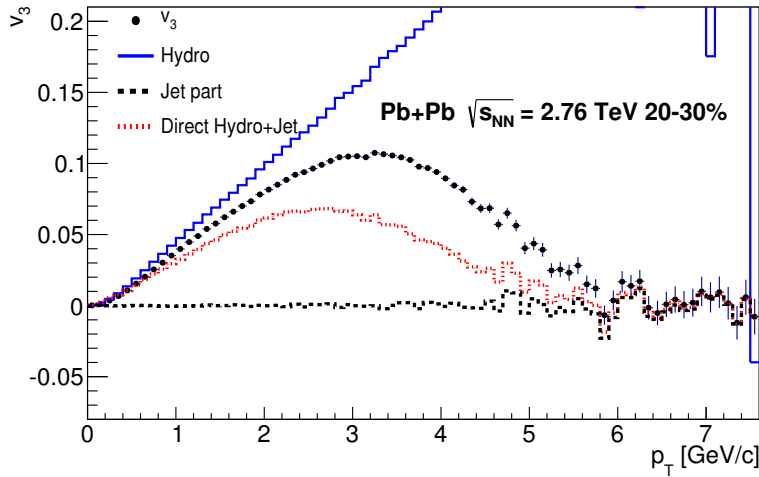
Figure 2. Transverse momentum distributions for v_3 calculated with HYDJET++ for charged particles in Pb+Pb at $\sqrt{s_{NN}} = 2.76$ TeV. Black circles show $v_3(p_T)$ for all charged particles, histograms represent flow coming from the hydrodynamics (blue solid line) and from jets (black dashed line) respectively. Red dotted histogram shows $v_3(p_T)$ for direct charged particles.
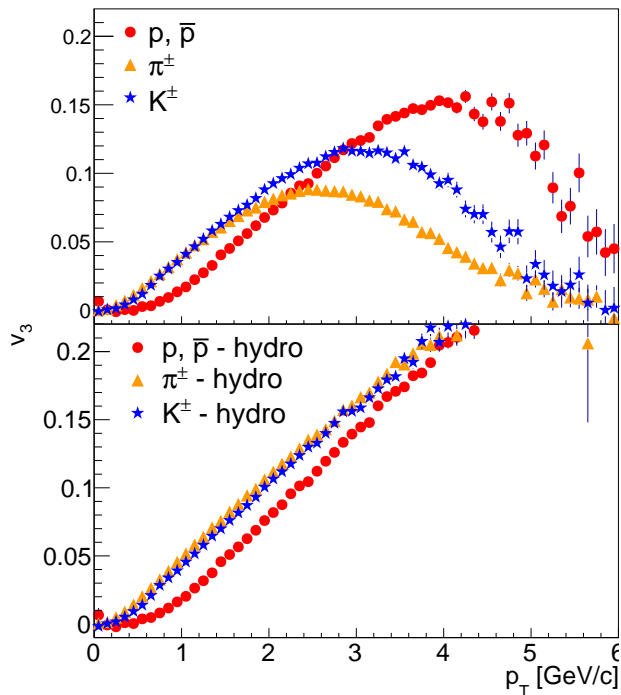
Figure 3. Top: Transverse momentum distribution of triangular flow $v_3(p_T)$ for all pions (yellow triangles), protons (red circles) and kaons (blue stars) in Pb+Pb at $\sqrt{s_{NN}} = 2.76$ TeV calculated with HYDJET++. Bottom: $v_3(p_T)$ distributions for pions, protons and kaons obtained from the hydrodynamical part within HYDJET++.

NCQ scaling of triangular flow at LHC was also studied. We considered the v_3 scaling as $v_3/n_q^{3/2}$, which was recently suggested by STAR [3]. Results for protons, kaons and pions are shown in Fig. 5 (a, b) for all hadrons and direct hadrons respectively. Plots (c, d) show the distributions (a, b) respectively divided by the corresponding distribution for proton. Proton and pion distributions seem to follow the scaling at low p_T, however the kaon distribution deviates by more than 50%. In case of direct hadrons, there is no evident scaling pattern as the pions do also deviate significantly already in the soft region.
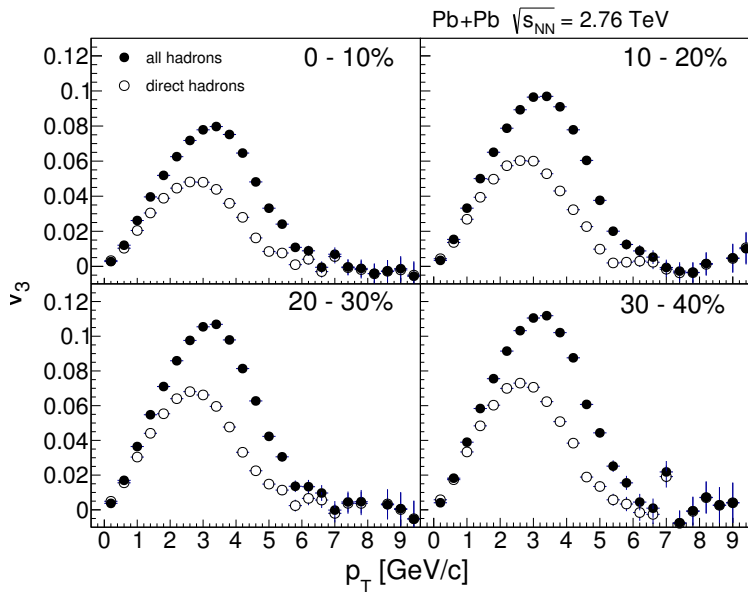
Figure 4. Triangular flow distribution $v_3(p_T)$ for all charged particles (full circles) and direct charged particles (open circles) in Pb+Pb at $\sqrt{s_{NN}} = 2.76$ TeV at centrality $0 - 40\%$.
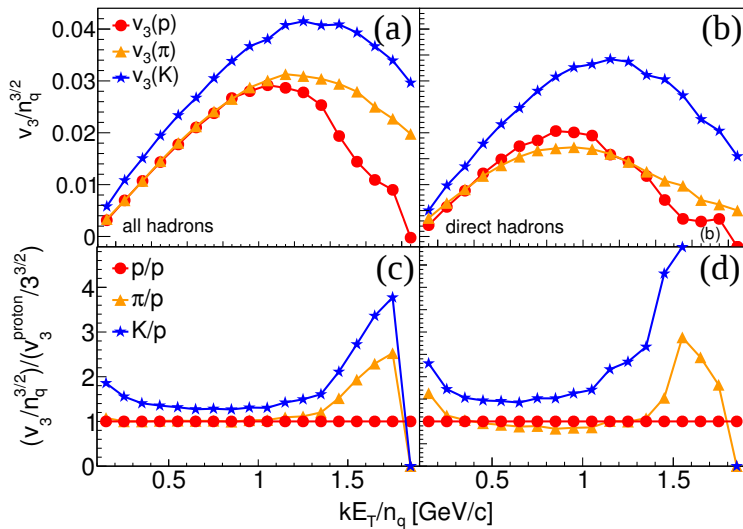
Figure 5. Number-of-constituent-quarks scaling for triangular flow in Pb+Pb at $\sqrt{s_{NN}} = 2.76$ TeV. Distributions for all protons (red circles), pions (yellow triangles) and kaons (blue stars) are shown in (a). The same for direct particles is in (b). The distributions of protons, pions and kaons divided by the proton distribution are depicted in (c), (d) shows the same for direct particles.

4 Conclusions

We performed a study of the effect of resonance decays on the triangular flow in Pb+Pb collisions within the HYDJET++ framework. The model provides a fair description of v_3 with centrality. It was found that resonances influence significantly the shape of flow distributions: for v_3 we observed in maximum a shift of about 10% to higher p_T and growth of about 40% in amplitude.

The number-of-constituent quark scaling is broken at LHC for v_3 as well as for v_2. However, the resonance decays drive the flow towards scaling.

It is vital to further study the flow of mother and daughter particles as well as influence of jets to better understand the dynamics of the system.

Acknowledgement

References

[1] K. Aamodt *et al.* (ALICE Collaboration), Phys. Rev. Lett 107 (2011) 032301.
[2] A. Adare *et al.* (PHENIX Collaboration), Phys. Rev. Lett 98 (2007) 162301.
[3] X. Sun (for STAR Collaboration), J. Phys.: Conf. Ser. 535 (2014) 012005.
[4] I. P. Lokhtin *et al.*, Comp. Phys. Comm. 180 (2009) 779–799.
[5] L. V. Bravina *et al.*, Eur. Phys. J. C 74 (2014) 2807.
[6] S. Chatrchyan *et al.* (CMS Collaboration), Phys. Rev. C 87 (2013) 014902.